Alzheimer disease and Parkinson disease patients. Genomics 17, 171–184.

Sian, J., Dexter, D.T., Jenner, P., Marsden, C.D., 1991. Decreased in nigral glutathione in Parkinson's disease. Br. J. Pharmacol. 104, 281.

Sulzer, D., Zecca, L., 2000. Intraneuronal dopamine-quinone synthesis: a review. Neurotox. Res. 1, 181–195.

Valente, E.M., Abou-Sleiman, P.M., Caputo, V., Muqit, M.M., Harvey, K., Gispert, S., Ali, Z., Del Turco, D., Bentivoglio, A.R., Healy, D.G., Albanese, A., Nussbaum, R., Gonzalez-Maldonado, R., Deller, T., Salvi, S., Cortelli, P., Gilks, W.P., Latchman, D.S., Harvey, R.J., Dallapiccola, B., Auburger, G., Wood, N.W., 2004. Hereditary early-onset Parkinson's disease caused by mutations in PINK1. Science 304, 1158–1160.

van der Walt, J.M., Nicodemus, K.K., Martin, E.R., Scott, W.K., Nance, M.A., Watts, R.L., Hubble, J.P., Haines, J.L., Koller, W.C., Lyons, K., Pahwa, R., Stern, M.B., Colcher, A., Hiner, B.C., Jankovic, J., Ondo, W.G., Allen, F.H. Jr., Goetz, C.G., Small, G.W., Mastaglia, F., Stajich, J.M., McLaurin, A.C., Middleton, L.T., Scott, B.L., Schmechel, D.E., Pericak-Vance, M.A., Vance, J.M., 2003. Mitochondrial polymorphisms significantly reduce the risk of Parkinson disease. Am. J. Hum. Genet. 72, 804–811.

Yamaguchi, H., Kajitani, K., Dan, Y., Furuichi, M., Ohno, M., Sakumi, K., Kang, D., Nakabeppu, Y., 2006. MTH1, an oxidized purine nucleoside triphosphatase, protects the dopamine neurons from oxidative damage in nucleic acids caused by 1-methyl-4-phenyl-1,2,3,6-tetrahydropyridine. Cell Death Differ. 13, 511–563.

Yoritaka, A., Hattori, N., Uchida, K., Tanaka, M., Stadtman, E.R., Mizuno, Y., 1996. Immunohistochemical detection of 4-hydroxynonenal protein adducts in Parkinson disease. Proc. Natl. Acad. Sci. USA 93, 2696–2701.

Zhang, J., Perry, G., Smith, M.A., Robertson, D., Olson, S.J., Graham, D.G., Montine, T.J., 1999. Parkinson's disease is associated with oxidative damage to cytoplasmic DNA and RNA in substantia nigra neurons. Am. J. Pathol. 154, 1423–1429.

Neuron
Article

Sept4, a Component of Presynaptic Scaffold and Lewy Bodies, Is Required for the Suppression of α-Synuclein Neurotoxicity

Masafumi Ihara,[1,*] Nobuyuki Yamasaki,[2] Akari Hagiwara,[1] Ai Tanigaki,[6] Ayumi Kitano,[1] Rie Hikawa,[1] Hidekazu Tomimoto,[3] Makoto Noda,[4] Masashi Takanashi,[5] Hideo Mori,[5] Nobutaka Hattori,[5] Tsuyoshi Miyakawa,[2] and Makoto Kinoshita[1,6,*]

[1]Biochemistry and Cell Biology Unit, HMRO, Kyoto University Graduate School of Medicine, Yoshida Konoe, Sakyo, Kyoto 606-8501, Japan

[2]Genetic Engineering and Functional Genomics Unit, HMRO, Kyoto University Graduate School of Medicine, Yoshida Konoe, Sakyo, Kyoto 606-8501, Japan

[3]Department of Neurology, Kyoto University Graduate School of Medicine, Yoshida Konoe, Sakyo, Kyoto 606-8501, Japan

[4]Department of Molecular Oncology, Kyoto University Graduate School of Medicine, Yoshida Konoe, Sakyo, Kyoto 606-8501, Japan

[5]Department of Neurology, Juntendo University School of Medicine, Hongo, Bunkyo, Tokyo 113-8431, Japan

[6]PRESTO, Japan Science and Technology Agency, Honcho, Kawaguchi, Saitama 332-0012, Japan

*Correspondence: ihara@kuhp.kyoto-u.ac.jp (M.I.), mkinoshita@hmro.med.kyoto-u.ac.jp (M.K.)

DOI 10.1016/j.neuron.2007.01.019

SUMMARY

In Parkinson disease (PD), α-synuclein aggregates called Lewy bodies often involve and sequester Septin4 (Sept4), a polymerizing scaffold protein. However, the pathophysiological significance of this phenomenon is unclear. Here, we show the physiological association of Sept4 with α-synuclein, the dopamine transporter, and other presynaptic proteins in dopaminergic neurons; mice lacking Sept4 exhibit diminished dopaminergic neurotransmission due to scarcity of these presynaptic proteins. These data demonstrate an important role for septin scaffolds in the brain. In transgenic mice that express human α-synuclein^{A53T} (a mutant protein responsible for familial PD), loss of Sept4 significantly enhances neuropathology and locomotor deterioration. In this PD model, insoluble deposits of Ser^{129}-phosphorylated α-synuclein^{A53T} are negatively correlated with the dosage of Sept4. In vitro, direct association with Sept4 protects α-synuclein against self-aggregation and Ser^{129} phosphorylation. Taken together, these data show that Sept4 may be involved in PD as a dual susceptibility factor, as its insufficiency can diminish dopaminergic neurotransmission and enhance α-synuclein neurotoxicity.

INTRODUCTION

Septins are polymerizing GTP binding proteins that serve as scaffolds for diverse molecules beneath the plasma membrane (Field and Kellogg, 1999; Versele and Thorner, 2005; Kinoshita, 2006). In addition to playing roles in mitosis (Kinoshita et al., 1997, Surka et al., 2002; Spiliotis et al., 2005), mammalian septins are abundant in the central nervous system (CNS) (Kinoshita et al., 1998, 2000; Xue et al., 2004; Hall et al., 2005), where they have been implicated in exocytosis (Hsu et al., 1998; Beites et al., 1999, 2005; Xue et al., 2004). However, it is not clear whether and how septins are involved in exocytosis and/or neurotransmission in vivo, partly because mice that lack *Sept3*, *Sept5*, or *Sept6* do not show obvious CNS abnormalities (Fujishima et al., 2007; Peng et al., 2002; Ono et al., 2005).

Meanwhile, septins have been implicated in diverse neurodegenerative disorders in humans. For instance, mutations in the *Sept9* gene were found in hereditary neuralgic amyotrophy (Kuhlenbaumer et al., 2005). Sept4 and two other septins were found in neurofibrillary tangles in Alzheimer's disease (Kinoshita et al., 1998). Sept4 coaggregates with α-synuclein in cytoplasmic inclusion bodies known as Lewy bodies (LBs) in sporadic Parkinson disease (PD) and dementia with Lewy bodies and in glial cytoplasmic inclusions in multiple system atrophy (Ihara et al., 2003). Sept4 and Sept5/CDCrel-1 are substrates for a ubiquitin ligase, parkin; hence, loss of parkin function may result in accumulation of these paralogous septins (Zhang et al., 2000b; Choi et al., 2003; Son et al., 2005). Intriguingly, acute overload of Sept5 can be both inhibitory to exocytosis and neurotoxic (Beites et al., 1999; Dong et al., 2003; Son et al., 2005). However, it is not clear whether the toxicity of septin overload or loss of septin function plays important roles in the pathogenesis of α-synucleinopathies.

This study was designed to address physiological and pathological roles of Sept4 in normal and PD brains. We first examined the status of Sept4 in sporadic PD cases and found that it was often deficient in dopaminergic

(DA) nerve terminals in the striatum. This prompted us to explore the consequences of Sept4 deficiency in *Sept4*$^{-/-}$ mice, and our comprehensive screening pinpointed a specific attenuation of their nigrostriatal DA transmission without affecting the neuronal morphology. We found that Sept4 is required for DA neurons to maintain key components of DA metabolism. Transgenic supplementation of Sept4 was sufficient to rescue the biochemical deficits in *Sept4*$^{-/-}$ striatum. Finally, we tested whether Sept4 deficiency could modify α-synucleinopathy in transgenic mice expressing human α-synuclein^{A53T}, a pathogenic mutant responsible for a trait of familial PD (Giasson et al., 2002). Surprisingly, genetic loss of *Sept4* in this PD model exacerbated neuronal loss, gliosis, and locomotor deterioration, which were accompanied by severe amyloid deposits containing Ser^{129}-phosphorylated α-synuclein^{A53T}. In vitro, Sept4 interfered with self-aggregation and Ser^{129} phosphorylation of α-synuclein. These results suggest that physiological interaction with Sept4 prevents α-synuclein from converting into neurotoxic species and aggregates, and that DA neurons deficient in Sept4 become more susceptible to further dysfunction and degeneration in PD.

RESULTS

Physiological Localization of Sept4 in Presynaptic Dopaminergic Terminals in Human Striatum and Its Depletion in Parkinson Disease

In agreement with our previous observations (Ihara et al., 2003), antibodies raised against three distinct epitopes of Sept4 consistently labeled LBs in the substantia nigra pars compacta (SNpc) of all sporadic PD cases examined (n = 5; Figures 1B and 1D, and data not shown). Sept4 and α-synuclein colocalized in the core of LBs (Figures 1C and 1D), indicating their close relationship. In contrast, antibodies for five other septins including Sept5/CDCrel-1 (a substrate for parkin) did not label LBs (Figure 1A and data not shown). These data confirmed the specific involvement of Sept4 in α-synuclein aggregates in PD.

In control human brains without PD, Sept4 was abundant in presynaptic terminals of DA neurons projecting from SNpc to the striatum (putamen). Sept4 was colocalized in the varicosities with the dopamine transporter (DAT in Figures 1E–1G) and α-synuclein (αS in Figures 1H–1J). These data suggest physiological association of Sept4 with these presynaptic molecules in DA nerve terminals.

To examine the status of presynaptic Sept4 in PD, we measured the content of Sept4 in the putamen by immunohistochemistry and immunoblot. In non-PD controls, immunohistochemical signals for Sept4 were more intense in the putamen than in the adjacent cerebral (insular) cortex (Figures 1K and 1S), while in PD, Sept4 was recognizably reduced in the putamen (Figures 1L and 1S). The deficiency of Sept4 was comparable with that of DAT in the adjacent slices (Figures 1Q and 1R). The relative densitometric values for Sept4 in the putamen (Dpu) and insular cortex (Dcx) could segregate PD cases from non-PD controls (Figure 1M, n = 12). In contrast, a general presynaptic marker, synaptophysin, was not reduced in PD putamen (Figures 1N–1P, n = 8). Consistently, immunoblot analysis demonstrated that Sept4 was often reduced in PD specifically in the putamen but not in the cerebral cortex (Figures 1T–1W and Figure S1 in the Supplemental Data). Considering the heterogeneous etiology of sporadic PD and the variability of individual human samples, Sept4 deficiency in the striatum is regarded as one of the common pathological changes in PD.

Loss of Sept4 Attenuates Dopaminergic Transmission in the Mouse

To address the physiological significance of Sept4 in the CNS, we examined the distribution of Sept4 and the impact of its loss in the mouse. Using in situ hybridization and immunohistochemistry techniques, it was demonstrated that Sept4 was expressed in specific cell populations in the cerebral cortex, striatum, midbrain, cerebellum, and spinal cord (Figures 2A–2E, Figure S9, and data not shown). As with DA neurons, Sept4 was present in the cell bodies in the SNpc and ventral tegmental area (VTA) (Figure 2D), in projection fiber bundles (arrows in Figures 2B and 2E), and in axon terminals surrounding striatal neurons (Figure 2E). As seen in the human brain, Sept4, α-synuclein, and DAT were abundant and colocalized in the axon terminals, especially at the varicosities (Figures 2F–2K).

We generated *Sept4*$^{-/-}$ mice with a genetic background of C57BL/6J, all of which appeared normal except for unexpected male infertility (Ihara et al., 2005). All the Sept4 polypeptides were abolished in *Sept4*$^{-/-}$ brain (Figures 2A–2C). Given the widespread distribution of Sept4 in the CNS, we performed a comprehensive physical and behavioral screening (Supplemental Figures S2–S5). *Sept4*$^{-/-}$ mice were normal except for a paradigm of prepulse inhibition of the acoustic startle response (PPI). This paradigm is an index of reduction in startle amplitude to a loud acoustic stimulus when the stimulus is preceded by a moderate prestimulus (Figure 3A). *Sept4*$^{-/-}$ mice exhibited a lower basal startle response and a significant enhancement in PPI (Figure 3B; p = 0.0011). Since DA antagonists can enhance PPI (Zhang et al., 2000a), we suspected attenuated DA transmission in *Sept4*$^{-/-}$ mice. The mice were challenged with apomorphine at a low dose (0.05 mg/kg) that is known to block DA transmission by selectively stimulating DA presynaptic autoreceptors (Starke et al., 1989). PPI was enhanced in *Sept4*$^{+/+}$ mice but disrupted in *Sept4*$^{-/-}$ mice (the differences between Figures 3B and 3C are indexed in Figure 3D). However, a higher dose of apomorphine (3 mg/kg), which dominantly stimulates postsynaptic DA receptors, disrupted PPI in both genotypes (Supplemental Figure S6). Thus, the attenuated DA transmission in *Sept4*$^{-/-}$ mice was attributed to presynaptic (rather than postsynaptic) defects.

To confirm this, we reassessed spontaneous locomotor activity in an open field (as in Supplemental Figure S5) with methamphetamine, which releases DA from the

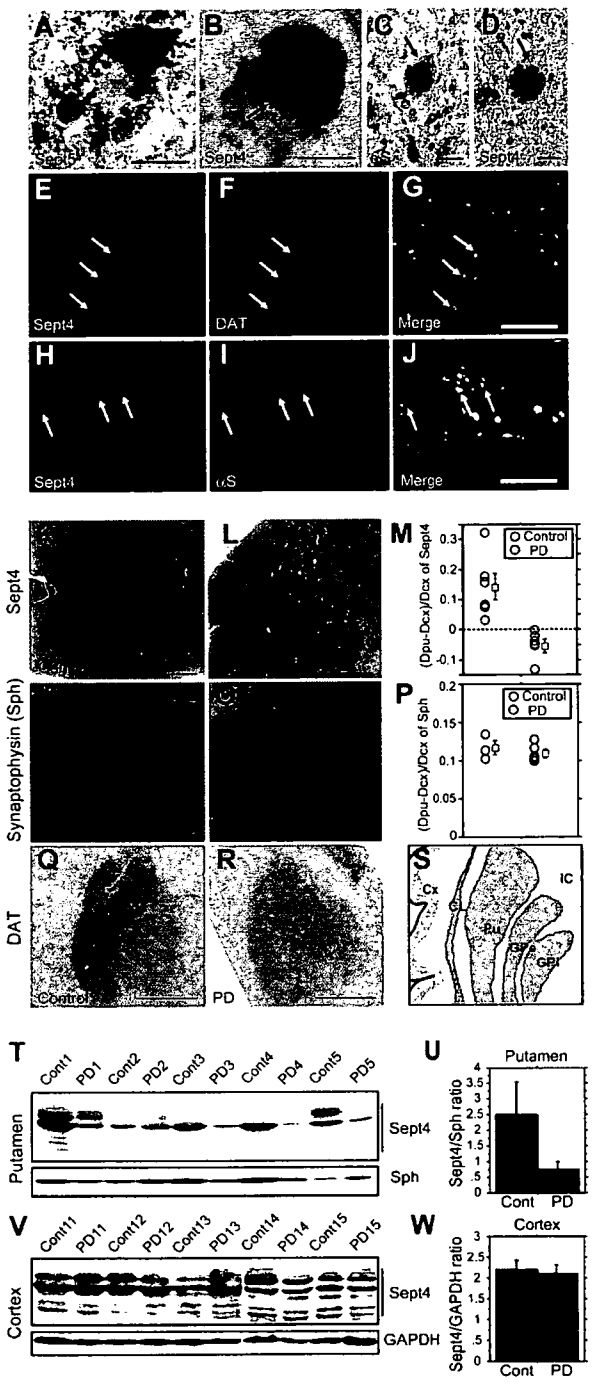

Figure 1. Involvement of Sept4 in Sporadic Parkinson Disease: Sequestration in Nigral Lewy Bodies and Depletion in the Striatum

(A and B) Nigral DA neurons bearing LBs in human brains affected with sporadic PD. LBs (arrows), surrounded by neuromelanin granules (dark brown deposits), were not labeled for Sept5 (A), but were consistently labeled for Sept4 (light brown signal in B). Bars, 20 μm.

(C and D) Two adjacent sections showing a DA neuron with an LB (arrows) containing both α-synuclein (αS) (C) and Sept4 (D). Bars, 20 μm.

(E–G) The normal human striatum labeled for Sept4 ([E], red) and the dopamine transporter (DAT) ([F], green) and the merged image [G]. Arrows indicate presynaptic varicosities where intense signals of Sept4 and DAT colocalize. Bar, 20 μm.

(H–J) The normal human striatum labeled for Sept4 ([H], red) and α-synuclein ([I], green) and the merged image (J). Sept4 also colocalized with α-synuclein in presynaptic varicosities (arrows). Bar, 20 μm.

(K and L) Representative images of Sept4 immunohistochemistry in coronally sectioned human brains without (K) and with (L) sporadic PD. Bars, 5 mm.

(M) Semiquantification of the Sept4 signal in the putamen with sporadic PD (n = 6) and without (n = 6). The relative abundance of Sept4 in the striatum is represented by an index, (Dpu-Dcx)/Dcx, where Dpu and Dcx are the densitometric values of Sept4 in the putamen and insular cortex, respectively.

(N–P) Relative striatal content of synaptophysin (Sph), a presynaptic marker protein, was analyzed as in (M). Unlike Sept4, synaptophysin was not depleted from the striatum in PD. Bars, 5 mm.

(Q and R) Immunohistochemistry of DAT in a non-PD (Q) and a PD (R) brain, showing depletion of DAT from the striatum in PD. Bars, 5 mm.

(S) An anatomical diagram of the human basal ganglia (coronal section). Cx, insular cortex; CL, claustrum; Pu, putamen; GPe/GPi, external/internal pallidum; IC, internal capsule.

(T and U) Relative content of Sept4 was quantified by immunoblot in the putamen of sporadic PD (n = 10) and non-PD (n = 10) brains. The densitometric ratio of Sept4/synaptophysin (Sph) was frequently reduced in the striata of the PD patients.

(V and W) Relative content of Sept4 was quantified by immunoblot in the frontal cortex of sporadic PD (n = 5) and non-PD (n = 5) brains. The densitometric ratio of Sept4/GAPDH was not reduced in the cerebral cortices of the PD patients. These data also exclude a possibility that Sept4 is subject to postmortem protein degradation.

presynaptic terminals (Hyman et al., 2006). While the basal activity and methamphetamine-driven hyperactive surge were almost normal in *Sept4*$^{-/-}$ mice, their hyperactivity decayed more rapidly (Figure 3E, $p < 0.05$). These data indicate a presynaptic cause of the attenuated DA transmission in *Sept4*$^{-/-}$ striatum.

In addition, DA content was significantly reduced in *Sept4*$^{-/-}$ striatum by ~25% (Figure 6G; $p = 0.039$), indicating a requirement of Sept4 for DA metabolism.

Dopaminergic Axon Terminals in *Sept4*$^{-/-}$ Striatum Are Morphologically Normal but Deficient in Key Molecules for Dopamine Metabolism

Based on the behavioral pharmacology data, we examined the status of nigral DA neurons by immunohistochemistry for tyrosine hydroxylase (TH), the rate-limiting enzyme of DA synthesis. In the midbrain, the number and morphology of TH-positive neuronal somata were comparable between *Sept4*$^{+/+}$ and *Sept4*$^{-/-}$ mice (Supplemental Figure S7). However, *Sept4*$^{-/-}$ striatum was labeled less intensely for TH and DAT (Figure 4A). Quantitative morphometric analyses of TH/DAT-positive axons and axon terminals at both the light microscopy level (Figure 4B) and EM level (Figure 4C and Supplemental Figure S8) could not discriminate the two genotypes.

In immunoblot, the densitometric ratios of TH and DAT against synapsin IIa or glyceraldehyde-3-phosphate dehydrogenase (GAPDH) were significantly reduced in *Sept4*$^{-/-}$ striatum (by ~30% and ~55%, respectively),

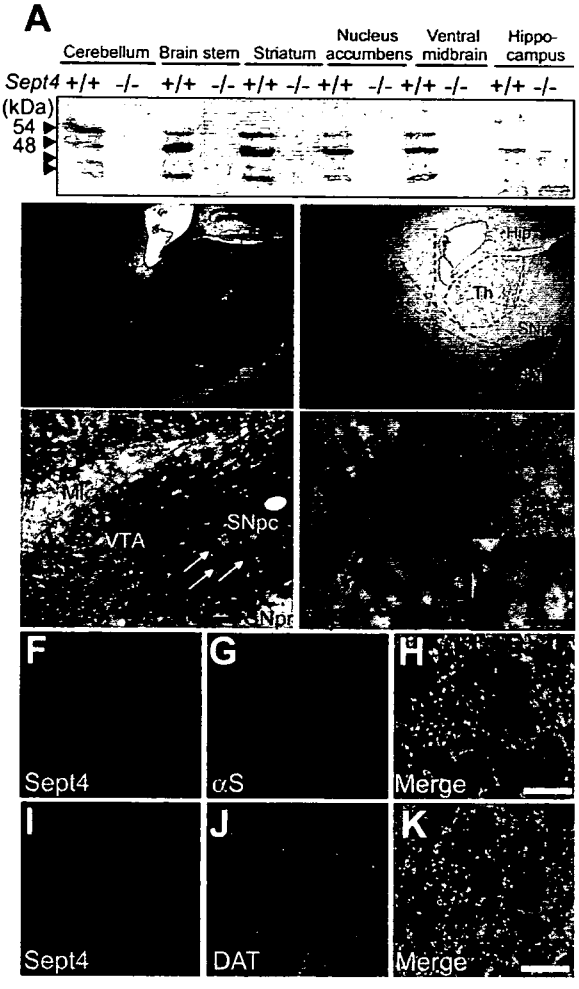

Figure 2. Expression of Sept4 in the Mouse Brain

(A) Immunoblot of mouse brain extracts for Sept4. Four *Sept4* products were detected in most parts of the brain to a varying degree and were abolished in *Sept4*$^{-/-}$ mice. Each lane contained 50 μg protein.

(B and C) Sept4 immunohistochemistry (brown signals) in parasagittal sections of *Sept4*$^{+/+}$ and *Sept4*$^{-/-}$ forebrains. The left and top in the figures are the rostral and dorsal aspects, respectively. Projection fiber bundles containing the nigrostriatal pathway are indicated by arrows in (B) and dotted arrows in (C). CCx, cerebral cortex; St, striatum; SNpc, substantia nigra pars compacta; SNpr, substantia nigra pars reticulata; Th, thalamus; Hip, hippocampus. Bars: 1.5 mm.

(D) Sept4 immunohistochemistry using nickel enhancement (blue signals) in a coronal section of *Sept4*$^{+/+}$ ventral midbrain. Sept4 was detected in neuronal cell bodies in the ventral tegmental area (VTA; black arrows) and SNpc (white arrows). MI, medial lemniscus. Bar: 20 μm.

(E) A parasagittal section of *Sept4*$^{+/+}$ striatum. Note Sept4-containing (brown) puncta in the axon bundles (arrows) and their terminals surrounding the target neurons (asterisks). Bar: 20 μm; inset, 10 μm.

(F–K) Double-label immunofluorescence of presynaptic terminals in *Sept4*$^{+/+}$ striatum. Sept4 signals ([F and I], red) were partially overlapped with those of α-synuclein ([G], green), and DAT ([J], green). Bars: 10 μm (H and K).

but not in the ventral midbrain (Figures 4D–4G; data not shown). However, five postsynaptic parameters we examined were unaffected (Figures 4H and 4I, Figure 6D, and data not shown). These data indicate that loss of Sept4 directly or indirectly reduces the concentration of TH and DAT in DA axons and axon terminals without affecting their morphology. The scarcity of the two essential molecules for DA metabolism may well account for the hypodopaminergic phenotype observed in *Sept4*$^{-/-}$ mice.

Transgenic Supplementation of Sept4 Can Restore the Deficiency of TH and DAT in *Sept4*$^{-/-}$ Mice

In the next series of experiments, we examined whether Sept4 can rescue the deficiency of TH and DAT in *Sept4*$^{-/-}$ mice. For these purposes, we generated two lines of transgenic mice, *Sept4-Tg1* and *Sept4-Tg2*, each harboring ~10 transcription units of *Sept4*$^{54\ kDa}$ cDNA driven by the prion promoter. The heterozygous Tg mice were lean (~25% body weight reduction), short-lived, and barely fertile. These defects seemed to be due to the nonspecific cytotoxicity of Sept4 overload (Ihara et al., 2003; Dong et al., 2003) and ectopic Sept4 expression in the heart, adrenal gland, and germ cells (see Discussion). Crossbreeding of *Sept4-Tg1* and *Sept4*$^{-/-}$ mice rarely generated live *Sept4KO/Tg1* mice that expressed Sept4$^{54\ kDa}$ and shorter processed forms in the striatum. *Sept4KO/Tg1* striatum contained normal levels of TH and DAT (Figures 5A and 5B). Although *Sept4KO/Tg2* mice were never born, *Sept4-Tg2* mice showed hyper-dopaminergic behaviors (Figures 5C and 5D) and supernormal levels of TH and DAT (data not shown).

Although the primary effects from the loss or excess of Sept4 may be complicated by compensatory and adaptive changes, these data consistently indicate a positive role for Sept4 in DA metabolism.

Sept4 Is Required as a Component of the Presynaptic Machinery for DA Turnover

To determine the molecular mechanism underlying the hypo-dopaminergic phenotype of *Sept4*$^{-/-}$ mice, we immunoprecipitated striatal homogenates of *Sept4*$^{+/+}$ mice with anti-Sept4 antibodies, then immunoblotted for possible Sept4-interacting molecules. Consistent with our previous report (Ihara et al., 2003) and the colocalization data (Figures 1G and 1J and Figures 2H and 2K), Sept4 was coimmunoprecipitated with DAT and α-synuclein (Figures 6A and 6B). Since Sept5, the closest paralog of Sept4, has been implicated in syntaxin (Stx)-mediated exocytosis (Beites et al., 1999), we tested the interaction between these septins and Stx-1A. Sept5 and Stx-1A were coimmunoprecipitated from the cerebellar cortex, but not from the striatum (data not shown). In contrast, Sept4 and Stx-1A were reciprocally coimmunoprecipitated from the striatum (Figures 6A and 6C). However, a component of the exocyst complex, Sec8, and a postsynaptic protein, mGluR1, were present in the striatum but did not immunoprecipitate with Sept4 (Figure 6A). These data indicate a physiological association of Sept4 with presynaptic molecules involved in DA release and reuptake. Given the individual associations between α-synuclein and DAT (Lee et al., 2001), and Stx-1A and DAT

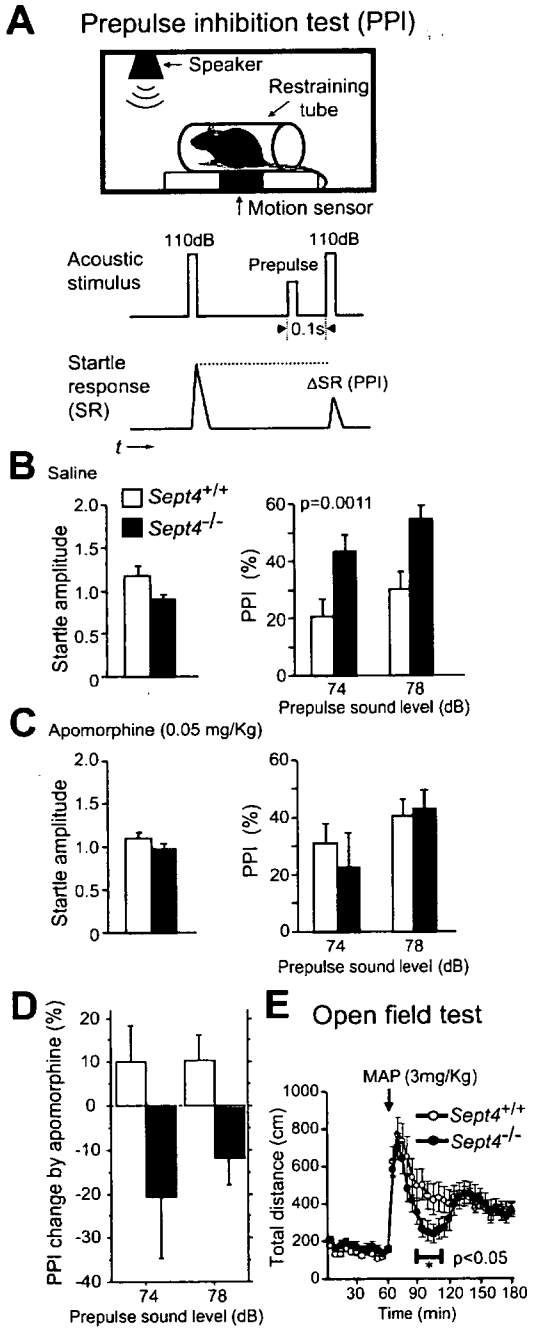

Figure 3. *Septin4*$^{-/-}$ Mice Exhibit Hypo-Dopaminergic Abnormalities in Prepulse Inhibition and Methamphetamine-Induced Locomotor Response

(A) (Top) The measurement of PPI of acoustic startle response. (Bottom) PPI is defined here as the percent reduction in the amplitude of the startle response to a loud stimulus (pulse) when it is preceded by a moderate prestimulus (prepulse).

(B) The startle response amplitude to a 110 dB stimulus (left) and PPI (right) after a mock pretreatment with saline. As compared with *Septin4*$^{+/+}$ littermates, *Septin4*$^{-/-}$ mice showed significant enhancement in PPI by a prepulse of 74 or 78 dB (n = 15 per genotype).

(C) The startle amplitude to the 110 dB stimulus (left) and PPI (right) after a pretreatment with a DA agonist, apomorphine (0.05 mg/Kg s.c.). Presynaptic DA blockade by apomorphine enhanced PPI in *Septin4*$^{+/+}$ mice (as seen in *Septin4*$^{-/-}$ mice in B), whereas it paradoxically disrupted PPI in *Septin4*$^{-/-}$ mice.

(D) Comparison of the apomorphine-induced PPI changes by genotype.

(E) Methamphetamine-induced hyperactivity was not sustained in *Septin4*$^{-/-}$ mice. Spontaneous activities of *Septin4*$^{+/+}$ and *Septin4*$^{-/-}$ littermates were automatically measured in an open field setup. After a habituation, methamphetamine (MAP, 3 mg/Kg, i.p.) was injected at $t = 60$ (min, arrow). Although the basal and peak activities of *Septin4*$^{-/-}$ mice were almost normal, locomotion was significantly less than that of *Septin4*$^{+/+}$ littermates for the time block of $t = 85$–110 ($F_{1,30} = 4.172$, $p < 0.05$, n = 16 per genotype). The activity of *Septin4*$^{-/-}$ mice recovered to the normal level at $t = 130$ and later.

(Lee et al., 2004), our results point to a larger protein complex in the striatum that contains Sept4, α-synuclein, Stx-1A, and DAT.

Septins often serve as scaffolds that anchor and/or stabilize other molecules. Depletion of cellular septins by RNAi reduces the amount of binding partners in the same complex (Kinoshita et al., 2002). Thus, we examined whether the loss of Sept4 also affects interaction partners other than DAT. In *Septin4*$^{-/-}$ striatum, the contents of Stx-1A, SNAP25, Munc18, and α-synuclein were slightly but consistently reduced, while that of Vesl-1L, a postsynaptic protein, was not affected (Figures 6D–6F). (Note: we predict the deficiencies of Stx-1A and α-synuclein in DA neurons were underestimated by this method; these molecules are also expressed in other cells that do not express Sept4, and are hence unaffected by the loss of Sept4.)

The biochemical evidence, along with the colocalization and behavioral data, strongly suggests that Sept4 is closely associated with the key molecules for DA metabolism. Considering the normal morphology of *Septin4*$^{-/-}$ DA neurons (Figures 4B and 4C and Supplemental Figure S8), Sept4 may be required not as a cytoskeletal protein, but as a component of a presynaptic scaffold that directly or indirectly supports the molecular machinery for dopamine turnover.

Loss of *Sept4* Exacerbates Neuropathology of *α-Synuclein*^{A53T} Transgenic Mice

Next, we focused on pathological interaction between Sept4 and another molecule in the DA terminals, α-synuclein. We have so far demonstrated their physiological association and pathological coaggregation in α-synucleinopathies (Ihara et al., 2003; and Figures 1B–1D, Figure 2H, and Figures 6A, 6B, 6D, and 6F). To critically test whether the interaction with Sept4 promotes or suppresses aggregation and neurotoxicity of α-synuclein, we utilized *Septin4*$^{-/-}$ mice. We also employed a transgenic mouse model of α-synucleinopathy, in which human α-synuclein^{A53T} (a mutant protein responsible for a trait of familial PD) is expressed by the prion promoter (Giasson et al., 2002). As reported, biallelic *α-synuclein*^{A53T} transgenic mice (αS^{tg} mice) developed locomotor deterioration,

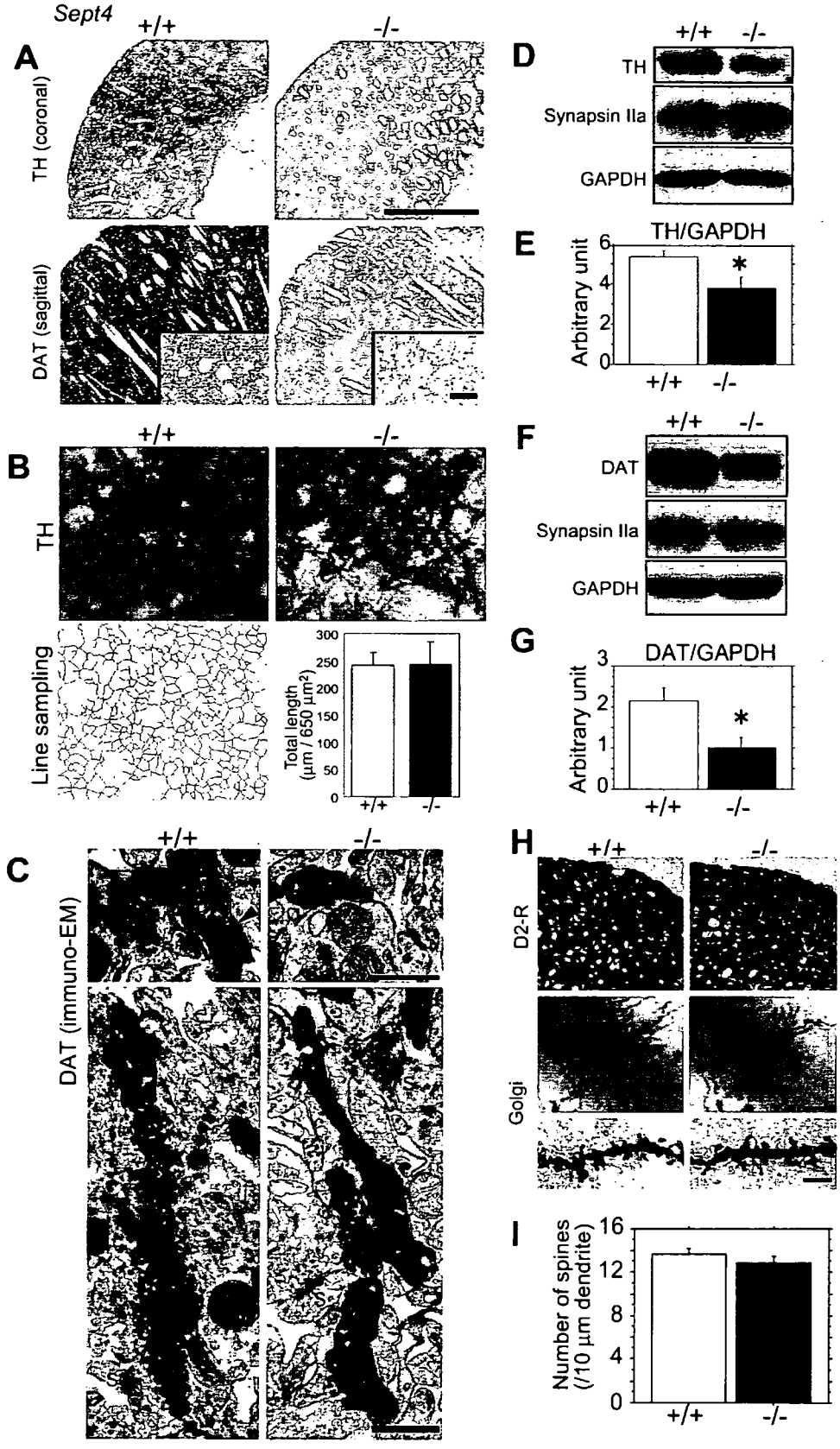
Sept4
+/+
-/-
A
TH (coronal)
DAT (sagittal)
B
TH
Line sampling
Total length (μm / 650 μm²)
C
DAT (immuno-EM)
D
TH
Synapsin IIa
GAPDH
E
TH/GAPDH
Arbitrary unit
F
DAT
Synapsin IIa
GAPDH
G
DAT/GAPDH
Arbitrary unit
H
D2-R
Golgi
I
Number of spines (/10 μm dendrite)

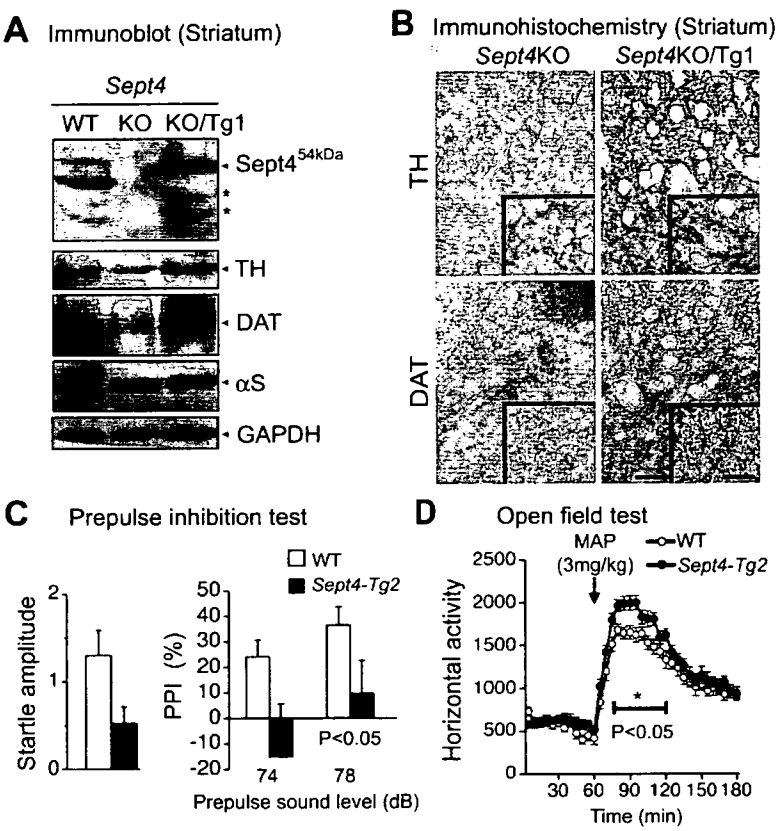

Figure 5. Transgenic Supplementation of Septa4$^{54\ kDa}$ Can Restore the Scarcity of Presynaptic Molecules in *Septa4*$^{-/-}$ Striatum

(A) Immunoblot showing the content of Sept4, TH, DAT, α-synuclein (αS), and GAPDH in the striatum of *Septa4*$^{+/+}$ (WT), *Septa4*$^{-/-}$ (KO), and *Septa4*$^{-/-}$/*Septa4*$^{54\ kDa}$ transgenic mice (KO/Tg1). Note that the scarcity of TH and DAT in *Septa4*$^{-/-}$ striatum was reversed by adding back the *Septa4*$^{54\ kDa}$ transgene. The asterisks indicate as of yet uncharacterized processed forms (probably amino-terminal truncations) of Septa4$^{54\ kDa}$. Each lane contained 50 μg protein.

(B) Immunohistochemistry for TH and DAT in the striatum of *Septa4*$^{-/-}$ (KO) and *Septa4*$^{-/-}$/*Septa4*$^{54\ kDa}$ (KO/Tg1) mice. The signal intensities were restored in DA terminals, most obviously in the presynaptic varicosities (compare also with Figures 4A and 4B). Bar: 20 μm; inset, 10 μm.

(C and D) Another line of transgenic mice, *Septa4-Tg2*, exhibited mild hyper-dopaminergic behaviors, i.e., disruption of PPI (C) and hypersensitivity to methamphetamine in the open field test (D). These behaviors, completely opposite to the hypo-dopaminergic phenotype of *Septa4*$^{-/-}$ mice, suggest that Sept4 is a positive determinant of DA neurotransmission.

i.e., hindlimb paralysis followed by quadriparesis, and died within a week after the onset of the symptom. All the symptomatic animals examined exhibited α-synuclein pathology throughout the neuraxis. Of note, Sept4 involvement in α-synuclein aggregates was visualized in this model of α-synucleinopathy (Figure 7A).

We examined consequences of genetic loss of *Sept4* in αS^{tg} mice. Unlike non-Tg mice that lived more than 24 months with or without *Sept4*, αS^{tg} mice lacking *Sept4* ($\alpha S^{tg}/S4^{-/-}$) had significantly shorter half survival time of ~12 months as compared with ~17 months of the original αS^{tg} ($\alpha S^{tg}/S4^{+/+}$) mice (Figure 7B, $p < 0.05$). As reported on the original αS^{tg} mice (Giasson et al., 2002), $\alpha S^{tg}/S4^{-/-}$ mice developed α-synuclein aggregates in the brainstem nuclei and spinal ventral horns (Figure 7C). Intriguingly, however, neuropathology of $\alpha S^{tg}/S4^{-/-}$ mice was distinct both qualitatively and quantitatively from that of $\alpha S^{tg}/S4^{+/+}$ mice in the following four ways.

(1) In the pontine reticular nuclei and spinal ventral horns, $\alpha S^{tg}/S4^{-/-}$ mice developed more amyloid deposits of α-synuclein that contained a pathologically phosphorylated form (pSer^{129}αS; Fujiwara et al., 2002) and were

Figure 4. Loss of Sept4 Attenuates Key Components of Dopamine Metabolism without Affecting the Morphology of DA Neurons

(A) Comparative immunohistochemistry revealed that the signal intensity for tyrosine hydroxylase (TH) and DAT were reduced in *Septa4*$^{-/-}$ striatum. Bar: 0.5 mm; inset, 20 μm.

(B) Network of axons and axon terminals of DA neurons were faintly labeled for TH but morphologically well-developed in *Septa4*$^{-/-}$ striatum. TH-positive structures were automatically extracted from digital microscopic images (e.g., bottom, left), and the total length of each binary image was quantified and statistically analyzed (bottom, right). There was no difference in the total length of TH-positive structures by genotype. See Experimental Procedures for details. Bar: 20 μm.

(C) Immuno-EM images for DAT in the dorsal striata of *Septa4*$^{+/+}$ and *Septa4*$^{-/-}$ mice. The fine morphology of DA neuron terminals was not different between genotypes. Some DAT-positive presynaptic terminals containing synaptic vesicles are apposed to postsynaptic densities (PSDs, arrowheads) formed in the medium spiny neurons. S, asymmetric nondopaminergic (probably glutamatergic) synapses. The total DAT-positive area measured on immuno-EM images was comparable between *Septa4*$^{+/+}$ and *Septa4*$^{-/-}$ striata (Supplemental Figure S8). Bar: 0.5 μm.

(D and E) Mild reduction of TH content in *Septa4*$^{-/-}$ striatum. Homogenates of *Septa4*$^{+/+}$ and *Septa4*$^{-/-}$ striata were blotted for TH, synapsin IIa, and GAPDH. The TH/GAPDH ratio was significantly reduced in *Septa4*$^{-/-}$ striatum ($p < 0.05$, $n = 5$ per genotype). Each lane contained 50 μg protein.

(F and G) As in (D) and (E), significant reduction of DAT content was confirmed in *Septa4*$^{-/-}$ striatum ($p < 0.01$, $n = 7$ per genotype), which is consistent with the immunohistochemical data in (A). Each lane contained 50 μg protein.

(H and I) In contrast, postsynaptic components were unaffected by the loss of *Septa4*. The intrinsic neurons in *Septa4*$^{-/-}$ striatum were morphologically normal in terms of the number of the medium spiny neurons (data not shown), immunohistochemistry for the dopamine type 2 receptor (D2R, [H]), Golgi impregnation stain (Golgi, [H]), and the density of dendritic spines (I). Bar: top panels, 0.1 mm; middle panels, 20 μm; bottom panels, 3 μm.

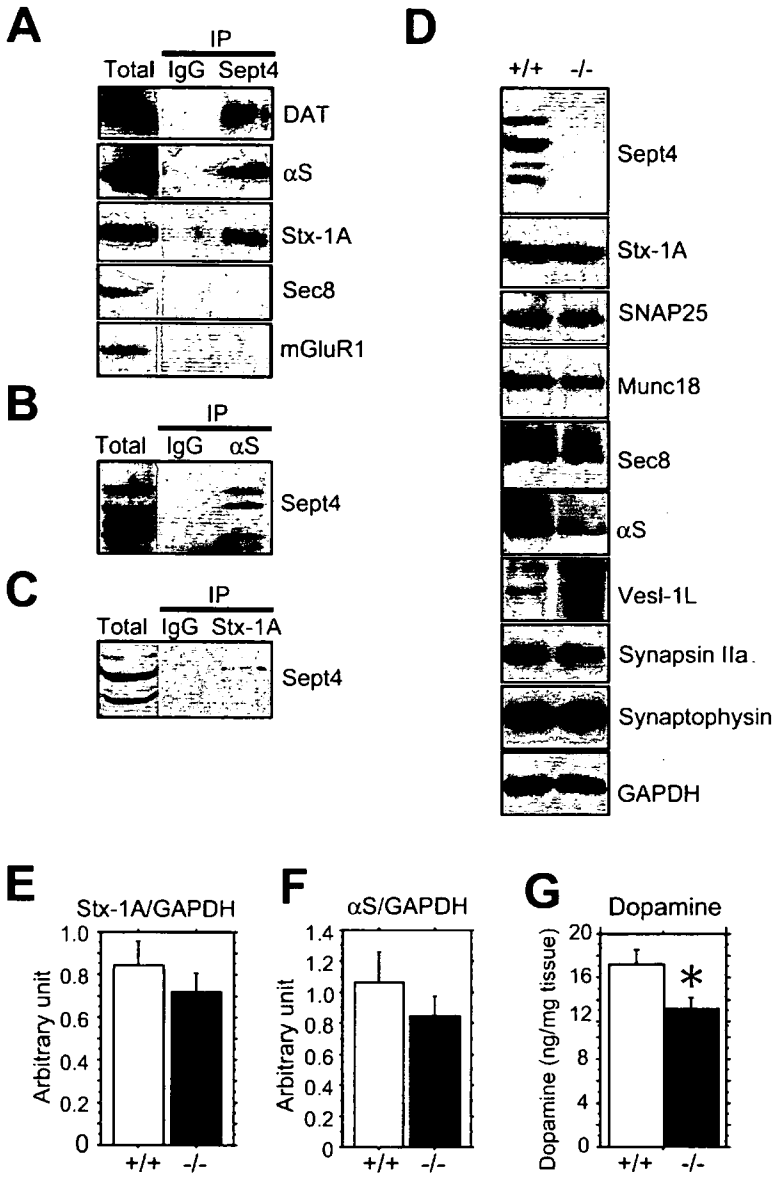

Figure 6. Selective Scarcity of Proteins for Dopamine Turnover and Dopamine in *Septa4*$^{-/-}$ Striatum

(A–C) Physical association of Sept4 with DAT, αS, and syntaxin (Stx)-1A in the striatum. (A) *Septa4*$^{+/+}$ striatal homogenate was immunoprecipitated with preimmune rabbit IgG (negative control) or the rabbit polyclonal antibody H5C2 for Sept4, and probed for proteins as indicated. (B and C) The same homogenate was immunoprecipitated with mouse IgG (negative control) and mouse monoclonal antibodies for αS (B) or Stx-1A (C), and probed for Sept4.

(D) Immunoblot of *Septa4*$^{+/+}$ (+/+) and *Septa4*$^{-/-}$ (−/−) striatal homogenates for pre- and postsynaptic proteins.

(E and F) The densitometric ratios of Stx-1A/GAPDH (E) and αS/GAPDH (F) were slightly reduced in *Septa4*$^{-/-}$ striata (n = 5 per genotype). Because Stx-1A and αS are ubiquitous in the brain, their scarcity in *Septa4*$^{-/-}$ DA terminals seems to be obscured.

(G) DA content measured by HPLC was significantly reduced in *Septa4*$^{-/-}$ striatum by 25% (p = 0.039, n = 5 per genotype). There was a similar trend in the nucleus accumbens, another target of nigral DA neurons (data not shown).

resistant to digestion by proteinase K (Figure 7C, top panels, and Supplemental Figure S11). (2) In the spinal ventral horns, *αS*^{tg}*/S4*$^{-/-}$ mice exhibited a significant loss of large motor neurons (>20 μm in diameter); however, smaller motor neurons and interneurons were not affected (~5–20 μm) (Figure 7C, bottom panels, and Figure 7D). (3) In the spinal ventral horns, *αS*^{tg}*/S4*$^{-/-}$ mice exhibited more severe astrocytic gliosis, indicative of ongoing inflammatory and degenerative processes (Supplemental Figure S10). (4) In the SNpc of *αS*^{tg}*/S4*$^{-/-}$ mice, pSer^{129}αS-positive aggregates were formed in DA neurons and swollen neurites (Figure 7F), and were not found in *αS*^{tg}*/S4*$^{+/+}$ mice. These data indicate that *Septa4* can be regarded as a suppressor of neurodegeneration by *α-synuclein*^{A53T} overload.

Septa4 Can Suppress Pathological Modifications of α-Synuclein In Vivo

To analyze the molecular basis of the enhancement of α-synuclein pathology by the loss of *Septa4*, we examined the biochemical status of α-synuclein in graded extraction (i.e., in Triton-soluble, sodium dodecyl sulfate- [SDS-] soluble, and SDS-insoluble fractions) of the spinal cord. In each fraction of young asymptomatic mice, α-synuclein was detected mainly as the native form of ~17 kDa (αS in Figure 7E, left top panel). Intriguingly, the SDS-insoluble fraction of aged, symptomatic mice additionally contained putative crosslinked dimers [$(αS)_2$] and other modified forms, high-molecular-weight smears (HMWαS), and aggregates that stuck at the top of the resolving gel (arrow in Figure 7E, right top panel). These aberrant α-synuclein

species were more prominent in symptomatic $\alpha S^{tg}/S4^{-/-}$ mice than in older symptomatic $\alpha S^{tg}/S4^{+/+}$ mice (compare the second and third lanes from the right in Figure 7E, right top panel). The modified α-synuclein species were reminiscent of those found in human α-synucleinopathies; i.e., the ~24 kDa band may correspond to *O*-glycosylation (Shimura et al., 2001) or another modification (Tofaris et al., 2003), and the ~40 kDa double bands may represent crosslinked homodimers and/or other modified species (Kahle et al., 2001). None of these modified species were labeled for ubiquitin (data not shown).

Among other biochemical abnormalities, accumulation of pSer^{129}αS in the SDS-insoluble fraction was the most significant characteristic of symptomatic $\alpha S^{tg}/S4^{-/-}$ mice (Figure 7E, right second panel). The amount of insoluble pSer^{129}αS was positively correlated with the severity of neuropathology in the spinal cord. Thus, SDS-insoluble pSer^{129}αS seems to correspond to the protease-resistant amyloid deposits (Figure 7C and Supplemental Figure S11). αS^{tg} mice hemizygous for *Sept4* ($\alpha S^{tg}/S4^{+/-}$) contained an intermediate amount of pSer^{129}αS in each fraction (Supplemental Figure S12), indicating that the dosage of Sept4 is a determinant of α-synuclein modification. Importantly, symptomatic $\alpha S^{tg}/S4^{-/-}$ mice contained SDS-insoluble pSer^{129}αS not only in the spinal cord, but also in the forebrain (data not shown) and the nigral DA neurons in the midbrain (Figures 7F–7H).

Taken together, aggregation and Ser^{129} phosphorylation of α-synuclein seem to be central events underlying the neurodegeneration of αS^{tg} mice, and these pathological modifications were obviously enhanced by the loss of Sept4.

Direct Interaction with Sept4 Prevents Self-Aggregation and Ser^{129} Phosphorylation of α-Synuclein In Vitro

How does Sept4 suppress neurotoxicity caused by chronic overload of α-synuclein? It has been hypothesized that self-aggregation of α-synuclein that occurs in various pathological processes generates neurotoxic species (Dawson and Dawson, 2003), and that Ser^{129} phosphorylation can facilitate the process (Fujiwara et al., 2002). Thus, we tested in vitro whether these modifications could be suppressed by Sept4. First, we confirmed that α-synuclein and Sept4 directly associate in vitro (Figure 8A). Second, we found that Sept4 suppressed self-aggregation of α-synuclein^{A53T} into SDS-resistant HMW species (Figure 8B). Third, Sept4 partially interfered with Ser^{129} phosphorylation of α-synuclein^{A53T} by a ubiquitous Ser/Thr-kinase, casein kinase II (CKII; Fujiwara et al., 2002) (Figure 8C). However, Sept4 did not essentially inhibit the kinase activity of CKII when casein was used as the substrate (Supplemental Figure S13). When the data were taken together, we concluded that direct interaction with Sept4 can prevent α-synuclein from self-aggregation (as has been proposed for another LB component, αB-crystallin) (Rekas et al., 2004), and may shield α-synuclein from Ser^{129} phosphorylation by CKII and other kinases. Such protective effects on α-synuclein modifications, perhaps by steric hindrance and/or conformational changes, may be more effective in the physiological situation where Sept4, DAT, and Stx-1A are in close proximity to α-synuclein (Figure 6A).

DISCUSSION

Sept4$^{-/-}$ Mice Revealed a Physiological Septin Function in the Brain

Septins have been implicated in exocytosis based on their presynaptic localization (Kinoshita et al., 2000; Xue et al., 2004), physical and functional interaction with syntaxins (Beites et al., 1999, 2005), and aberrant exocytosis in blood platelets lacking Sept5 (Dent et al., 2002). However, previous attempts to address septin functions in the brain with *Sept3*$^{-/-}$, *Sept5*$^{-/-}$, or *Sept6*$^{-/-}$ mice were unsuccessful, probably due to compensation by their functionally redundant paralogs (Fujishima et al., 2007; Peng et al., 2002; Ono et al., 2005). We employed a comprehensive behavioral test as a means of unbiased screening for neurological defects in *Sept4*$^{-/-}$ mice. This approach has successfully pinpointed a specific neurological phenotype by the loss of septin function, i.e., the attenuation of nigrostriatal DA transmission. While DA neurons were functionally affected by the loss of Sept4, non-DA neurons were unchanged. This intriguing form of selectivity may be due to the absence of redundant septin species, and/or a specific requirement of Sept4 subunit, in DA neurons.

Sept4 Is Required as a Component of Presynaptic Scaffolds in DA Neurons

Extending our previous finding of Sept4 involvement in LBs (Ihara et al., 2003), the present study has revealed Sept4 insufficiency in presynaptic DA terminals in the human striatum affected with sporadic PD. This is partly due to sequestration of Sept4 into α-synuclein aggregates, and partly as a result of neuronal loss. To investigate the pathophysiological impact of Sept4 depletion in PD, we created and investigated several mouse models: the genetic loss of *Sept4* attenuated, an excess of Sept4 enhanced, and a transgenic Sept4 supplementation of *Sept4* null mice normalized nigrostriatal DA transmission. These results suggest a positive role for Sept4 in dopamine turnover.

The hypo-dopaminergic behavioral deficits observed in *Sept4*$^{-/-}$ mice were attributed not to morphological anomalies of DA neurons but to an insufficiency of specific components in DA terminals. The levels of DAT, TH, α-synuclein, Stx-1A, and another tSNARE component depended more or less on the amount of Sept4. Sept4 directly or indirectly interacts with most of these molecules in the striatum. Considering the physical association of these molecules, Sept4 can be regarded as a pivotal component of the presynaptic scaffold for the machinery of dopamine release and reuptake. The detailed organization of such machinery would be an intriguing subject for future studies.

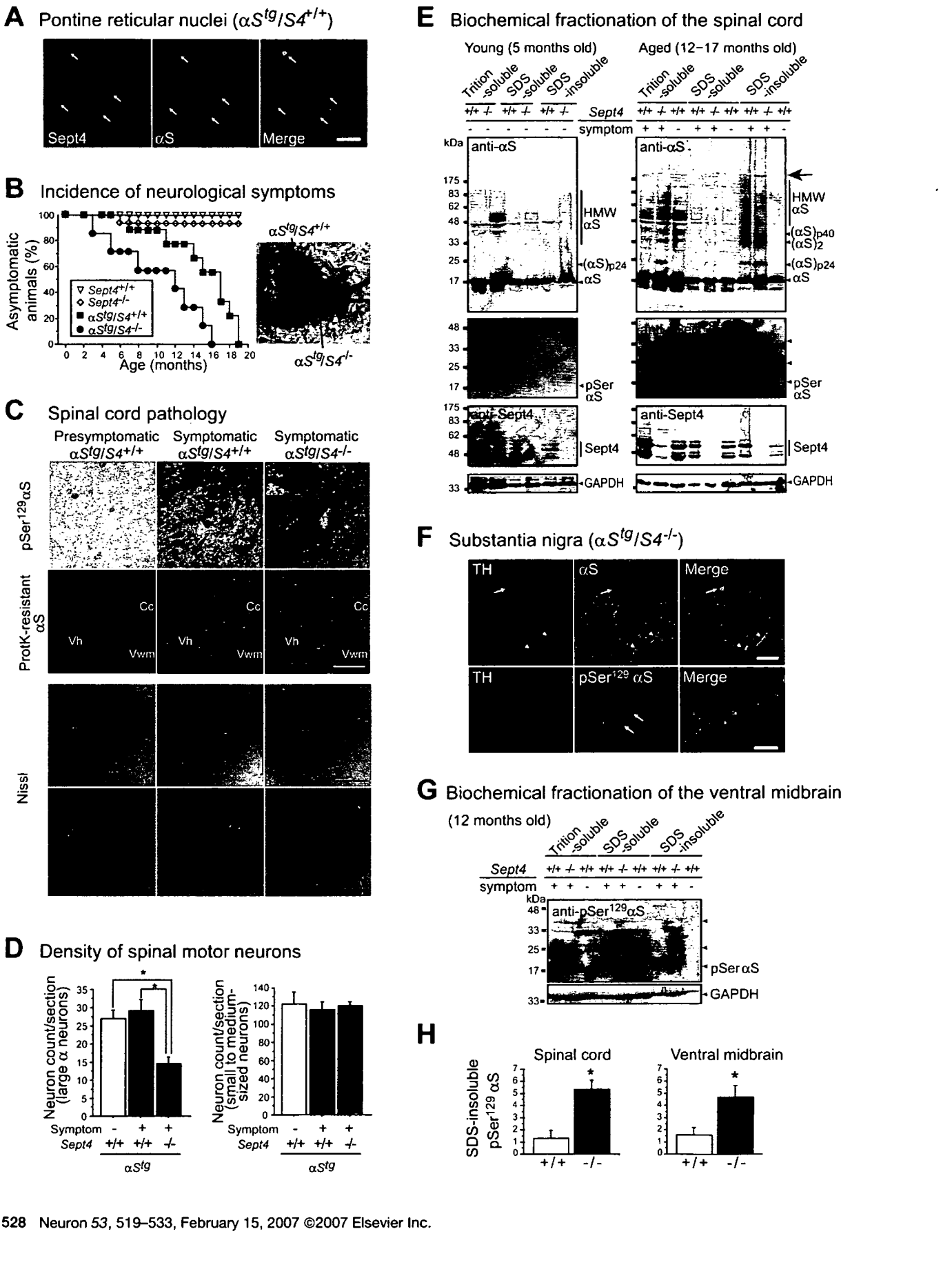
A Pontine reticular nuclei ($\alpha S^{tg}/S4^{+/+}$)
Sept4
αS
Merge
B Incidence of neurological symptoms
Asymptomatic animals (%)
Age (months)
Sept4+/+
Sept4-/-
αStg/S4+/+
αStg/S4-/-
αStg/S4+/+
αStg/S4-/-
C Spinal cord pathology
Presymptomatic αStg/S4+/+
Symptomatic αStg/S4+/+
Symptomatic αStg/S4-/-
pSer129αS
ProtK-resistant αS
Nissl
Cc
Vh
Vwm
D Density of spinal motor neurons
Neuron count/section (large α neurons)
Neuron count/section (small to medium-sized neurons)
Symptom
Sept4
αStg
E Biochemical fractionation of the spinal cord
Young (5 months old)
Aged (12–17 months old)
Trition -soluble
SDS -soluble
SDS -insoluble
Sept4
symptom
kDa
anti-αS
HMW αS
(αS)p24
αS
(αS)p40
(αS)2
anti-pSer αS
pSer αS
anti-Sept4
Sept4
GAPDH
F Substantia nigra ($\alpha S^{tg}/S4^{-/-}$)
TH
αS
Merge
pSer129 αS
G Biochemical fractionation of the ventral midbrain
(12 months old)
anti-pSer129αS
pSerαS
GAPDH
H
SDS-insoluble pSer129 αS
Spinal cord
Ventral midbrain
+/+
-/-

Physiological and Pathological Interaction between Sept4 and α-Synuclein

α-Synuclein, a presynaptic protein of unknown physiological function, is a soluble, natively unfolded polypeptide. Our study demonstrated physical interaction between α-synuclein and Sept4 in presynaptic terminals of nigral DA neurons. A recent report proposed that α-synuclein might act as a molecular chaperone for some tSNARE components, as excessive α-synuclein prevented the presynaptic degeneration in $CSP\alpha^{-/-}$ mice (Chandra et al., 2005). The close association of Sept4 with both α-synuclein and tSNAREs suggests that Sept4 is involved in the proposed scheme. The similar hypo-dopaminergic phenotypes observed in $Sept4^{-/-}$ and $\alpha\text{-}synuclein^{-/-}$ mice (Abeliovich et al., 2000) also support a functional convergence of these molecules.

Under pathological conditions where α-synuclein is overloaded and/or displaced in DA neurons, the polypeptide is subject to various modifications. Above all, Ser^{129} phosphorylation commonly found in LBs/Lewy neurites is considered the hallmark of α-synucleinopathies because $pSer^{129}\alpha S$ is absent in normal presynaptic terminals and prone to form aggregates in vitro (Fujiwara et al., 2002). Our data suggest that Sept4 and α-synuclein are components of presynaptic complexes at the DA terminals, and that lack of the physiological association with Sept4 facilitates self-aggregation and Ser^{129} phosphorylation of α-synuclein.

How Is Sept4 Involved in α-Synucleinopathy?

This study demonstrated that αS^{tg} and $\alpha S^{tg}/S4^{-/-}$ mice provide important insights into the biochemical processes underlying α-synucleinopathies. We have demonstrated that endogenous Sept4 is involved in α-synuclein aggregates formed in αS^{tg} mice (Figure 7A) as well as humans with sporadic PD (Ihara et al., 2003; Figure 1B–1D). The increased α-synuclein aggregation in $\alpha S^{tg}/S4^{-/-}$ mice indicates that Sept4 incorporation is a secondary event that can suppress further α-synuclein aggregation. Based on these and other findings, we propose a model for α-synucleinopathies (Figure 8D), whereby incipient α-synuclein aggregates formed in DA neurons adsorb Sept4. This may retard LB formation, but it eventually depletes Sept4 from the presynaptic terminals (Figure 1K–1U). As seen in $\alpha S^{tg}/S4^{-/-}$ mice, Sept4 insufficiency attenuates DA transmission and subjects α-synuclein to toxic conversions. Thus, pathological α-synuclein/Sept4 interaction in LBs and dissociation of their physiological interaction at presynaptic terminals may constitute a vicious cycle that further disrupts homeostasis of DA neurons in PD.

Figure 7. Loss of Sept4 Exacerbates Neuropathology and Aberrant α-Synuclein Modifications in $\alpha\text{-}synuclein^{A53T}$ Transgenic Mice

(A) Representative α-synuclein aggregates formed in a symptomatic $\alpha S^{tg}/S4^{+/+}$ mouse, 12 months old (m.o.). Coaggregation of Sept4 (red) with αS (green), as seen in human LBs, is recapitulated in this model of α-synucleinopathy. Bar, 20 μm.

(B) (Left) A chart showing the age of onset of hindlimb paresis in αS^{tg} mice with or without *Sept4*. The $Sept4^{+/+}$ and $Sept4^{-/-}$ non-Tg mice (green and pink plots, respectively) never showed the symptom. Intriguingly, however, $\alpha S^{tg}/S4^{-/-}$ mice (red) developed hindlimb paresis and died 3–4 months earlier than the original $\alpha S^{tg}/S4^{+/+}$ mice (blue; Giasson et al., 2002). (Right) A 12 m.o. $\alpha S^{tg}/S4^{+/+}$ presymptomatic mouse rearing on its $\alpha S^{tg}/S4^{-/-}$ littermate, which had developed hindlimb paresis (arrows).

(C) (First and second panels from top) Representative images of the spinal ventral horn comparatively immunostained for $pSer^{129}\alpha S$ (brown) or labeled for total αS after proteinase K digestion (green fluorescence). Each inset shows a $pSer^{129}\alpha S$-positive large motor neuron in the ventral horn (arrowheads); compare the levels of $pSer^{129}\alpha S$ and misfolded αS deposits in a 12 m.o. presymptomatic $\alpha S^{tg}/S4^{+/+}$ mouse (left panels), a 16 m.o. symptomatic $\alpha S^{tg}/S4^{+/+}$ mouse (middle panels), and a 12 m.o. symptomatic $\alpha S^{tg}/S4^{-/-}$ mouse (right panels). Bar: upper panels, 40 μm; lower panels, 200 μm. Vh, ventral horn; Vwm, ventral white matter; Cc, central canal. (Third and fourth panels from top) Representative Nissl-stained sections of the spinal cord from the same animals. Note a recognizable reduction of large motor neurons in the symptomatic $\alpha S^{tg}/S4^{-/-}$ mouse (right panels). Bar: upper panels, 200 μm; lower panels, 60 μm.

(D) The counts of large neurons (left) and small to medium-sized neurons (right) in the spinal cord sections from presymptomatic $\alpha S^{tg}/S4^{+/+}$ mice (white bars, 5–8 m.o.), symptomatic $\alpha S^{tg}/S4^{+/+}$ mice (blue bars, 12–18 m.o.), and symptomatic $\alpha S^{tg}/S4^{-/-}$ mice (red bars, 10–14 m.o.). Note that large neurons, classified as α motor neurons, were selectively and significantly lost in $\alpha S^{tg}/S4^{-/-}$ mice ($^*p < 0.05$, n = 4 per genotype).

(E) (Left, top) The spinal cord homogenates of young presymptomatic $\alpha S^{tg}/S4^{+/+}$ and $\alpha S^{tg}/S4^{-/-}$ littermates were fractionated into Triton (X-100)-soluble, SDS-soluble, and SDS-insoluble components. Each fraction was immunoblotted for total αS, $pSer^{129}\alpha S$, Sept4, and GAPDH. The SDS-insoluble fraction of $\alpha S^{tg}/S4^{-/-}$ mice consistently contained low- to high-molecular-weight (HMW) smear of αS (rightmost lane). (Left, second panel) At this age, αS was barely Ser^{129} phosphorylated in any fraction/genotype measured. Thus, Ser^{129} phosphorylation is preceded by some other modifications that cause the mobility shift of αS. (Right, top) Likewise, $\alpha S^{tg}/S4^{+/+}$ (17 m.o.) and $\alpha S^{tg}/S4^{-/-}$ (12 m.o.) mice with or without symptoms were analyzed. In addition to prominent HMW smears of αS, the SDS-insoluble fractions of the symptomatic animals of each genotype contained larger aggregates at the top of the resolving gel (arrow) and above in the stacking gel. However, only symptomatic $\alpha S^{tg}/S4^{-/-}$ mice contained heavy bands of modified αS (p40, crosslinked dimer, p24; arrowheads) in the SDS-insoluble fraction. (Right, second panel) The aged symptomatic animals commonly contained $pSer^{129}\alpha S$ in the Triton-soluble and SDS-soluble fractions. In addition, symptomatic $\alpha S^{tg}/S4^{-/-}$ mice contained significant $pSer^{129}\alpha S$ (monomer and higher molecular weight species; arrowheads) in the SDS-insoluble fraction. (Right, third panel) Sept4 in the SDS-insoluble fraction was increased and smeared in symptomatic $\alpha S^{tg}/S4^{+/+}$ mice, reflecting some biochemical modifications and coaggregation with αS.

(F) Double-label immunofluorescence for TH (red) and αS or $pSer^{129}\alpha S$ (green) in $\alpha S^{tg}/S4^{-/-}$ SNpc. αS/$pSer^{129}\alpha S$-positive aggregates in DA neurons, which were reminiscent of LBs (arrows) and Lewy neurites (arrowheads), were often found in $\alpha S^{tg}/S4^{-/-}$ ventral midbrain, but never in $\alpha S^{tg}/S4^{+/+}$ mice (data not shown). Bars: upper panels, 40 μm; lower panels, 20 μm.

(G) The ventral midbrains (containing DA neurons in SNpc and VTA) were analyzed as in (E). Intriguingly, each fraction of symptomatic $\alpha S^{tg}/S4^{-/-}$ mice contained more $pSer^{129}\alpha S$ (monomer and higher molecular weight species; arrowheads) than that of $\alpha S^{tg}/S4^{+/+}$ mice.

(H) Experiments of (E) and (G) were triplicated and quantified. The densitometric ratio of $pSer^{129}\alpha S$/GAPDH in the SDS-insoluble fraction was significantly higher in the spinal cord and ventral midbrain of symptomatic $\alpha S^{tg}/S4^{-/-}$ mice (−/−) as compared with symptomatic $\alpha S^{tg}/S4^{+/+}$ mice (+/+; $^*p < 0.01$, n = 3).

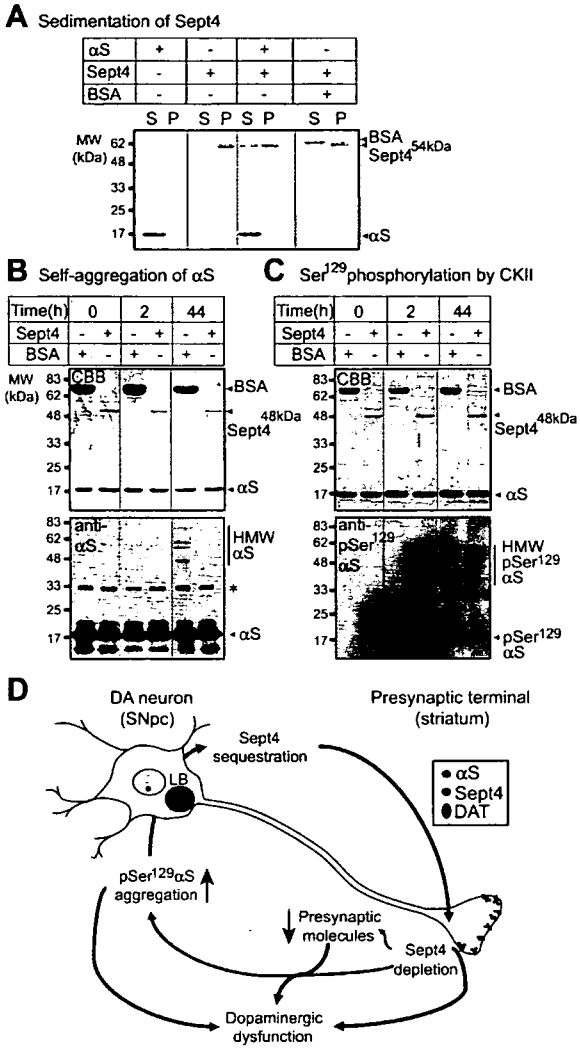

Figure 8. Sept4 Directly Interacts with α-Synuclein and Suppresses Its Self-Aggregation and Ser^{129} Phosphorylation In Vitro

(A) Sept4 directly interacts with αS. Mixtures of αS (wild-type), Sept4$^{54\ kDa}$, or BSA in PBS were ultracentrifuged at 440,000 × g for 30 min. The supernatant (S) and the pellet (P) of each mixture were analyzed by SDS-PAGE and stained with Coomassie Brilliant Blue (CBB). (From left to right lanes) αS alone was soluble (S). Most of Sept4 was sedimented (P), perhaps due to homo-oligomerization. αS interacted with Sept4 and interfered with the sedimentation. BSA, another soluble protein used as a control, did not show such effects. These data indicate direct association between Sept4 and αS.

(B) Sept4 can suppress self-aggregation of αS in vitro. (Top and middle panels) Recombinant human α-synuclein^{A53T} (αS) was incubated in a physiological buffer with recombinant Sept4$^{48\ kDa}$ or BSA. Each reaction was resolved by SDS-PAGE and CBB stained. (Bottom panel) The same reactions were immunobloted for total αS. After 44 hr incubation without Sept4, a fraction of αS was self-aggregated or oligomerized as HMW bands. In contrast, HMW bands of αS were not formed in the presence of Sept4. A 34 kDa band (*) represents αS dimers formed in *E.coli* (Masuda et al., 2006).

(C) Sept4 can mildly interfere with casein kinase II (CKII)-mediated phosphorylation and other modifications of α-synuclein in vitro. (Top and middle panels) αS^{A53T}, CKII, and ATP were incubated in a buffer with recombinant Sept4$^{48\ kDa}$ or BSA, and analyzed as in (A). (Bottom panel) The same reactions were immunobloted for pSer^{129}αS. Sept4 mildly interfered with Ser^{129}phosphorylation of αS^{A53T} and the formation of HMW species containing pSer^{129}αS. These data also suggested that pSer^{129}αS is more prone to self-aggregation than αS (compare the rightmost lanes of B and C). Parallel reactions using wild-type αS (instead of αS^{A53T}) gave similar results (data not shown). Data in (A)–(C) are representative of at least three experiments.

(D) A working model of PD pathophysiology including Sept4 as a novel player: α-synuclein aggregates (LB) formed by various pathological causes commonly involve Sept4. The involvement may retard the process while it sequesters and depletes Sept4 from DA nerve terminals in the striatum. The insufficiency of Sept4 in the presynaptic scaffold reduces the critical components for DA transmission, which contributes to DA dysfunction. In addition, an excess of α-synuclein in the absence of Sept4 facilitates its oligomerization, phosphorylation, and other modifications, which generate neurotoxic species.

Intriguingly, DA neurons in αS^{tg} mice developed α-synuclein aggregates only in the absence of Sept4 (Figures 7F–7H). Thus, loss of Sept4 is a critical event for the development of α-synuclein pathology in DA neurons, although it appears additional insults and/or aging are necessary for them to die. When compared with mice, human DA neurons are more sensitive to various insults, including α-synuclein overload (LaVoie et al., 2005; Moore et al., 2005). Thus, Sept4 depletion found in humans (Figures 1K–1U) should impact DA neurons more seriously.

Loss of Sept4 Function versus Gain of Toxic Effects

Sept4-Tg1 and *Sept4-Tg2* transgenic mice generated in this study have demonstrated that mild chronic overload of Sept4 is cytotoxic to various cell lineages. This is consistent with previous findings that acute Sept5 overexpression can damage DA neurons in the rat (Dong et al., 2003). Thus, both insufficiency and excess of Sept4 could perturb the homeostasis of DA neurons, ultimately leading to disorganization of their presynaptic terminals—another intriguing similarity to α-synuclein (Abeliovich et al., 2000; Chandra et al., 2005; Moore et al., 2005). As for sporadic PD cases, however, we have not obtained any samples that contained excessive Sept4 in the striatum. Thus, Sept4 overload may not be relevant in the etiology of sporadic PD.

In summary, our present as well as previous studies have established physiological and pathological roles of Sept4 in the nigral DA neurons. Future studies should characterize the presynaptic complex containing Sept4 and other key molecules. From a pathological aspect, unraveling the precise molecular mechanism by which Sept4 suppresses the α-synuclein toxicity may help develop neuroprotective strategies for PD.

EXPERIMENTAL PROCEDURES

Analyses of Clinical Samples

Postmortem human brain tissues were dissected within 6 hours postmortem under signed informed consent from the patients' relatives, and in accordance with the guidelines of ethics committees of Kyoto University and Juntendo University. Tissues for immunohistochemistry were fixed at Kyoto University Hospital. Donor subjects included 16 PD

patients (age range, 62–87 years old [y.o.]; mean, 73.7 y.o.) and 16 patients who died of nonneurological diseases (47–94 y.o.; mean, 64.1 y.o.). The frontal cortex and striatal tissues for immunoblot were dissected at Kyoto University Hospital and Juntendo Hospital, respectively, quickly frozen, and preserved at −80°C until protein extraction (see Supplemental Figure S1 for clinical data). In each case, the clinical diagnosis was confirmed neuropathologically, mostly by the presence of nigral LBs by hematoxylin-eosin stain. For immunohistochemistry, the brains fixed with 4% paraformaldehyde were sliced coronally, and the cerebral region containing the basal ganglia was isolated and embedded in paraffin, sectioned (6 μm thick), and subjected to immunohistochemistry as previously described (Ihara et al., 2003). The immunostained sections were optically scanned (16 bit, 600 dpi), and the integrated densities for a selected area (2 mm × 2 mm) were calculated with software (MultiGauge 2.0, Fujifilm, Japan). In each sample, three or more areas of the putamen and insular cortex were measured to obtain the average densitometric values.

Double-Label Immunofluorescence

Double-labeling immunofluorescence studies were performed by incubating human and mouse tissue sections with anti-Sept4, -DAT, or -α-synuclein antibodies. Fluorescein isothiocyanate- or rhodamine-conjugated appropriate secondary antibodies were applied. See the Supplemental Data for details.

Comparative Morphometric Analyses of DA Nerve Terminals at Light Microscopy and EM Levels

High-contrast images of TH-stained mouse striatal sections were captured and digitized by a light microscope with a CCD camera. The digital images were binarized with an arbitrary threshold, and the total length of the TH-positive neurites was calculated using Neurocyte Image Analyzer, ver. 1.5 (Kurabo, Japan). For the EM-level measurement of DA nerve terminal area, we used immuno-EM images of TH and DAT. TH- or DAT-positive areas in each digital EM image displayed on a computer screen were encircled manually using a digital pen tablet system, Intuos3 (Wacom Technology, Japan). The total encircled area was automatically calculated with graphic software (Scion, ver. β 4.0.2.). For each marker, 24 fields from corresponding regions of dorsal striata of *Sept4*$^{+/+}$ and *Sept4*$^{-/-}$ littermates were randomly sampled and analyzed blindly.

Immunoblotting and Immunoprecipitation

For immunoblotting, striatal tissues punched out from coronal brain slices of 3–5 m.o. mice were homogenized and sonicated in buffer A (10 mM Tris-HCl [pH 7.6], 1% Triton X-100, 0.15 M NaCl, 0.1% sodium deoxycholate, 0.1% sodium dodecyl sulfate), and then centrifuged at 15,000 × g at 4°C for 0.5 hr. The protein content of the supernatants was quantified using the Bradford method, and 50 μg of protein was denatured with an equal volume of 2 × SDS sample buffer and subjected to a standard immunoblot assay using peroxidase-conjugated secondary antibodies and an ECL chemiluminescence kit (GE Healthcare Biosciences). The amount of immunoreactive proteins was estimated by densitometry (see above). For coimmunoprecipitation of proteins, tissues were extracted with buffer B (0.1 M Tris-HCl [pH 7.6], 1% Triton X-100, 0.1% sodium deoxycholate, 0.1% SDS, protease inhibitors). After centrifugation, the supernatants were diluted with nine volumes of lysis buffer B′ without Triton X-100, resulting in a final concentration of 0.1%. Each lysate was incubated with various antibodies and Affi-Prep Protein A beads (Bio-Rad) at 4°C for 1 hr. Immunoprecipitates on the beads were washed five times with lysis buffer A, and analyzed by immunoblot.

Animals and Experimental Design

All animal procedures were performed in accordance with the guidelines of the Animal Use and Care Committee of Kyoto University. Heterozygous *Sept4*$^{+/-}$ mice were backcrossed with C57BL/6J for at least ten generations (Ihara et al., 2005). *Sept4*$^{-/-}$ mice and the control littermates were generated from *Sept4*$^{+/-}$ mice. The original αS^{tg} mice were bred with *Sept4*$^{-/-}$ mice to generate $\alpha S^{tg}/S4^{+/-}$ mice, which were inbred to generate $\alpha S^{tg}/S4^{+/+}$, $\alpha S^{tg}/S4^{+/-}$, and $\alpha S^{tg}/S4^{-/-}$ littermates. Biallelic Tg mice were identified by real-time PCR analysis and verified by backcrossing. All comparisons were made between littermates to minimize confounding effects by different genetic backgrounds. All behavioral tests were carried out on male mice (2–2.5 m.o.) (Miyakawa et al., 2001). Mice were given a light/dark cycle of 12 hr (lights on at 7 a.m.) and food and water ad libitum. Behavioral testing was performed between 9 a.m. and 6 p.m. except for the home cage social interaction test. After each test, all apparatuses were cleaned with acidic hypochlorous solution that eliminated mouse odors. Mouse brains were dissected after deep anesthesia with sodium pentobarbital (50 mg/kg, i.p.) with or without transcardial perfusion with 0.01 M phosphate-buffered saline (PBS). For histological analysis, mice were additionally perfused with 4% paraformaldehyde and 0.2% picric acid in 0.1 M PBS. Tissues from symptomatic αS^{tg} mice were dissected within a few days after the onset of hindlimb paresis to prevent suffering for ethical reasons and to minimize temporal changes that might influence the results.

Biochemical Fractionation of Neural Tissues by Graded Extraction

The forebrain, brainstem, and spinal cord from $\alpha S^{tg}/S4^{+/+}$ or $\alpha S^{tg}/S4^{-/-}$ mice (5–16 m.o.) were dissected, weighed, and homogenized by sonication in 3 ml/g of buffer C (10 mM Tris-HCl [pH 7.6], 0.15 M NaCl, 1% Triton X-100, and protease inhibitors). The supernatant, after centrifugation at 15,000 × g at 4°C for 0.5 hr, was labeled as "Triton-soluble fraction." The pellet was sonicated and re-extracted with 1 ml/g of buffer D (10 mM Tris-HCl [pH 8.0], 0.15 M NaCl, 1% Triton X-100, 0.5% sodium deoxycholate, and 0.1% SDS) and fractionated by centrifugation at 15,000 × g at 4°C for 0.5 hr, and the supernatant was labeled as "SDS-soluble fraction." The pellet was dissolved by sonication and boiling in buffer E (3% SDS and 5% β-mercaptoethanol, 1 ml/g pellet), and the lysate was termed "SDS-insoluble fraction." The amounts proportional to the original brain weight were loaded on separate lanes and each fraction was analyzed by immunoblot.

In Vitro Sedimentation, Aggregation, and Phosphorylation Assays

The recombinant His_6-tagged mouse Sept4$^{54\ kDa}$ was prepared in Sf9 cells (Kinoshita et al., 2002). For recombinant mouse Sept4$^{48\ kDa}$, GST-fusion protein was expressed in *E.coli* with a plasmid, pGEX-6P (GE Healthcare Biosciences). After purification of GST-Sept4$^{48\ kDa}$ with glutathione-agarose beads, GST-PreScission protease (Roche) was added to the beads to cleave the GST tag and release untagged Sept4$^{48\ kDa}$. For sedimentation assay, 20 μl reactions of recombinant human αS (wild-type, 4 μg, BioMol), recombinant mouse Sept4$^{54\ kDa}$ (2 μg), and/or BSA (2 μg, Sigma) in PBS were incubated at 4°C for 16 hr. Each reaction was ultracentrifuged at 4°C at 440,000 × g for 30 min. The supernatants and the pellets were analyzed by SDS-PAGE/CBB. For self-aggregation and phosphorylation assays, recombinant human αS (A53T mutant, 100 μg, BioMol) was incubated in 100 μl reactions of 30 mM Tris-HCl (pH 7.5) and BSA (100 μg, Sigma) or recombinant Sept4$^{48\ kDa}$ (20 μg) at 37°C. For phosphorylation assays, 4 mM $MgCl_2$, 2 mM ATP, and CKII (500 U, New England Biolabs) were added. The reactions sampled at 0, 2, and 44 hr were analyzed by SDS-PAGE/CBB, and analyzed by immunoblot for αS or pSer^{129}αS.

Supplemental Data

The Supplemental Data for this article can be found online at http://www.neuron.org/cgi/content/full/53/4/519/DC1/.

ACKNOWLEDGMENTS

We thank R. Takahashi, Y. Mizuno, T. Iwatsubo, and Y. Kaziro for suggestions and encouragements; V.M.-Y. Lee and J.Q. Trojanowski for

the generous gift of *α-synuclein*^{A53T} transgenic mice; D.R. Borchelt for the prion promoter; S. Yamada for the generation of *Sept4-Tg* mice; A. Kinoshita, Y. Fukazawa, and R. Shigemoto for technical advice; and A. Khundakar for critical reading of our manuscript. This study was supported in part by Special Coordination Funds for Promoting Science and Technology; Grants-in-Aid from MEXT of Japan, PRESTO from JST, and Takeda Science Foundation (to M.K.); a postdoctoral fellowship from JSPS; and a Grant from the Ichiro Kanehara Memorial Foundation (to M.I.).

Received: May 26, 2006
Revised: December 11, 2006
Accepted: January 10, 2007
Published: February 14, 2007

REFERENCES

Abeliovich, A., Schmitz, Y., Farinas, I., Choi-Lundberg, D., Ho, W.H., Castillo, P.E., Shinsky, N., Verdugo, J.M., Armanini, M., Ryan, A., et al. (2000). Mice lacking alpha-synuclein display functional deficits in the nigrostriatal dopamine system. Neuron *25*, 239–252.

Beites, C.L., Xie, H., Bowser, R., and Trimble, W.S. (1999). The septin CDCrel-1 binds syntaxin and inhibits exocytosis. Nat. Neurosci. *2*, 434–439.

Beites, C.L., Campbell, K.A., and Trimble, W.S. (2005). The septin Sept5/CDCrel-1 competes with alpha-SNAP for binding to the SNARE complex. Biochem. J. *385*, 347–353.

Chandra, S., Gallardo, G., Fernandez-Chacon, R., Schluter, O.M., and Sudhof, T.C. (2005). Alpha-synuclein cooperates with CSPalpha in preventing neurodegeneration. Cell *123*, 383–396.

Choi, P., Snyder, H., Petrucelli, L., Theisler, C., Chong, M., Zhang, Y., Lim, K., Chung, K.K., Kehoe, K., D'Adamio, L., et al. (2003). SEPT5_v2 is a parkin-binding protein. Brain Res. Mol. Brain Res. *117*, 179–189.

Dawson, T.M., and Dawson, V.L. (2003). Molecular pathways of neurodegeneration in Parkinson's disease. Science *302*, 819–822.

Dent, J., Kato, K., Peng, X.R., Martinez, C., Cattaneo, M., Poujol, C., Nurden, P., Nurden, A., Trimble, W.S., and Ware, J.A. (2002). A prototypic platelet septin and its participation in secretion. Proc. Natl. Acad. Sci. USA *99*, 3064–3069.

Dong, Z., Ferger, B., Paterna, J.C., Vogel, D., Furler, S., Osinde, M., Feldon, J., and Büeler, H. (2003). Dopamine-dependent neurodegeneration in rats induced by viral vector-mediated overexpression of the parkin target protein, CDCrel-1. Proc. Natl. Acad. Sci. USA *100*, 12438–12443.

Field, C.M., and Kellogg, D. (1999). Septins: cytoskeletal polymers or signalling GTPases? Trends Cell Biol. *9*, 387–394.

Fujishima, K., Kiyonari, H., Kurisu, J., Hirano, T., and Kengaku, M. (2007). Targeted disruption of Sept3, a heteromeric assembly partner of Sept5 and Sept7 in axons, has no effect on developing CNS neurons. J. Neurochem., in press.

Fujiwara, H., Hasegawa, M., Dohmae, N., Kawashima, A., Masliah, E., Goldberg, M.S., Shen, J., Takio, K., and Iwatsubo, T. (2002). alpha-Synuclein is phosphorylated in synucleinopathy lesions. Nat. Cell Biol. *4*, 160–164.

Giasson, B.I., Duda, J.E., Quinn, S.M., Zhang, B., Trojanowski, J.Q., and Lee, V.M. (2002). Neuronal alpha-synucleinopathy with severe movement disorder in mice expressing A53T human alpha-synuclein. Neuron *34*, 521–533.

Hall, P.A., Jung, K., Hillan, K.J., and Russell, S.E. (2005). Expression profiling the human septin gene family. J. Pathol. *206*, 269–278.

Hsu, S.C., Hazuka, C.D., Roth, R., Foletti, D.L., Heuser, J., and Scheller, R.H. (1998). Subunit composition, protein interactions, and structures of the mammalian brain sec6/8 complex and septin filaments. Neuron *20*, 1111–1122.

Hyman, S.E., Malenka, R.C., and Nestler, E.J. (2006). Neural mechanisms of addiction: The role of reward-related learning and memory. Annu. Rev. Neurosci. *29*, 565–598.

Ihara, M., Tomimoto, H., Kitayama, H., Morioka, Y., Akiguchi, I., Shibasaki, H., Noda, M., and Kinoshita, M. (2003). Association of the cytoskeletal GTP-binding protein Sept4/H5 with cytoplasmic inclusions found in Parkinson's disease and other synucleinopathies. J. Biol. Chem. *278*, 24095–24102.

Ihara, M., Kinoshita, A., Yamada, S., Tanaka, H., Tanigaki, A., Kitano, A., Goto, M., Okubo, K., Nishiyama, H., Ogawa, O., et al. (2005). Cortical organization by the septin cytoskeleton is essential for structural and mechanical integrity of mammalian spermatozoa. Dev. Cell *8*, 343–352.

Kahle, P.J., Neumann, M., Ozmen, L., Muller, V., Odoy, S., Okamoto, N., Jacobsen, H., Iwatsubo, T., Trojanowski, J.Q., Takahashi, H., et al. (2001). Selective insolubility of alpha-synuclein in human Lewy body diseases is recapitulated in a transgenic mouse model. Am. J. Pathol. *159*, 2215–2225.

Kinoshita, A., Kinoshita, M., Akiyama, H., Tomimoto, H., Akiguchi, I., Kumar, S., Noda, M., and Kimura, J. (1998). Identification of septins in neurofibrillary tangles in Alzheimer's disease. Am. J. Pathol. *153*, 1551–1560.

Kinoshita, A., Noda, M., and Kinoshita, M. (2000). Differential localization of septins in the mouse brain. J. Comp. Neurol. *428*, 223–239.

Kinoshita, M. (2006). Diversity of septin scaffolds. Curr. Opin. Cell Biol. *18*, 54–60.

Kinoshita, M., Kumar, S., Mizoguchi, A., Ide, C., Kinoshita, A., Haraguchi, T., Hiraoka, Y., and Noda, M. (1997). Nedd5, a mammalian septin, is a novel cytoskeletal component interacting with actin-based structures. Genes Dev. *11*, 1535–1547.

Kinoshita, M., Field, C.M., Coughlin, M.L., Straight, A.F., and Mitchison, T.J. (2002). Self- and actin-templated assembly of mammalian septins. Dev. Cell *3*, 791–802.

Kuhlenbaumer, G., Hannibal, M.C., Nelis, E., Schirmacher, A., Verpoorten, N., Meuleman, J., Watts, G.D., De Vriendt, E., Young, P., Stogbauer, F., et al. (2005). Mutations in SEPT9 cause hereditary neuralgic amyotrophy. Nat. Genet. *37*, 1044–1046.

LaVoie, M.J., Ostaszewski, B.L., Weihofen, A., Schlossmacher, M.G., and Selkoe, D.J. (2005). Dopamine covalently modifies and functionally inactivates parkin. Nat. Med. *11*, 1214–1221.

Lee, F.J., Liu, F., Pristupa, Z.B., and Niznik, H.B. (2001). Direct binding and functional coupling of alpha-synuclein to the dopamine transporters accelerate dopamine-induced apoptosis. FASEB J. *15*, 916–926.

Lee, K.H., Kim, M.Y., Kim, D.H., and Lee, Y.S. (2004). Syntaxin 1A and receptor for activated C kinase interact with the N-terminal region of human dopamine transporter. Neurochem. Res. *29*, 1405–1409.

Masuda, M., Dohmae, N., Nonaka, T., Oikawa, T., Hisanaga, S., Goedert, M., and Hasegawa, M. (2006). Cysteine misincorporation in bacterially expressed human alpha-synuclein. FEBS Lett. *580*, 1775–1779.

Miyakawa, T., Yamada, M., Duttaroy, A., and Wess, J. (2001). Hyperactivity and intact hippocampus-dependent learning in mice lacking the M1 muscarinic acetylcholine receptor. J. Neurosci. *21*, 5239–5250.

Moore, D.J., West, A.B., Dawson, V.L., and Dawson, T.M. (2005). Molecular pathophysiology of Parkinson's disease. Annu. Rev. Neurosci. *28*, 57–87.

Ono, R., Ihara, M., Nakajima, H., Ozaki, K., Kataoka-Fujiwara, Y., Taki, T., Nagata, K., Inagaki, M., Yoshida, N., Kitamura, T., et al. (2005). Disruption of Sept6, a fusion partner gene of Mixed Lineage Leukemia (MLL), does not affect the ontogeny, leukemogenesis induced by MLL-SEPT6, or the phenotype induced by the loss of Sept4. Mol. Cell. Biol. *25*, 10965–10978.

Peng, X.R., Jia, Z., Zhang, Y., Ware, J., and Trimble, W.S. (2002). The septin CDCrel-1 is dispensable for normal development and neurotransmitter release. Mol. Cell. Biol. *22*, 378–387.

Rekas, A., Adda, C.G., Andrew Aquilina, J., Barnham, K.J., Sunde, M., Galatis, D., Williamson, N.A., Masters, C.L., Anders, R.F., Robinson, C.V., et al. (2004). Interaction of the molecular chaperone alphaB-crystallin with alpha-synuclein: effects on amyloid fibril formation and chaperone activity. J. Mol. Biol. *340*, 1167–1183.

Shimura, H., Schlossmacher, M.G., Hattori, N., Frosch, M.P., Trockenbacher, A., Schneider, R., Mizuno, Y., Kosik, K.S., and Selkoe, D.J. (2001). Ubiquitination of a new form of alpha-synuclein by parkin from human brain: implications for Parkinson's disease. Science *293*, 263–269.

Son, J.H., Kawamata, H., Yoo, M.S., Kim, D.J., Lee, Y.K., Kim, S., Dawson, T.M., Zhang, H., Sulzer, D., Yang, L., et al. (2005). Neurotoxicity and behavioral deficits associated with Septin5 accumulation in dopaminergic neurons. J. Neurochem. *94*, 1040–1053.

Spiliotis, E.T., Kinoshita, M., and Nelson, W.J. (2005). A mitotic septin scaffold required for mammalian chromosome congression and segregation. Science *307*, 1781–1785.

Starke, K., Gothert, M., and Kilbinger, H. (1989). Modulation of neurotransmitter release by presynaptic autoreceptors. Physiol. Rev. *69*, 864–989.

Surka, M.C., Tsang, C.W., and Trimble, W.S. (2002). The mammalian septin MSF localizes with microtubules and is required for completion of cytokinesis. Mol. Biol. Cell. *13*, 3532–3545.

Tofaris, G.K., Razzaq, A., Ghetti, B., Lilley, K.S., and Spillantini, M.G. (2003). Ubiquitination of alpha-synuclein in Lewy bodies is a pathological event not associated with impairment of proteasome function. J. Biol. Chem. *278*, 44405–44411.

Versele, M., and Thorner, J. (2005). Some assembly required: yeast septins provide the instruction manual. Trends Cell Biol. *15*, 414–424.

Xue, J., Tsang, C.W., Gai, W.P., Malladi, C.S., Trimble, W.S., Rostas, J.A., and Robinson, P.J. (2004). Septin 3 (G-septin) is a developmentally regulated phosphoprotein enriched in presynaptic nerve terminals. J. Neurochem. *91*, 579–590.

Zhang, J., Forkstam, C., Engel, J.A., and Svensson, L. (2000a). Role of dopamine in prepulse inhibition of acoustic startle. Psychopharmacology (Berl.) *149*, 181–188.

Zhang, Y., Gao, J., Chung, K.K., Huang, H., Dawson, V.L., and Dawson, T.M. (2000b). Parkin functions as an E2-dependent ubiquitin-protein ligase and promotes the degradation of the synaptic vesicle-associated protein, CDCrel-1. Proc. Natl. Acad. Sci. USA *97*, 13354–13359.

Available online at www.sciencedirect.com
ScienceDirect
Neuroscience Research 60 (2008) 120–127
Neuroscience Research
www.elsevier.com/locate/neures

Technical note

Wireless voltammetry recording in unanesthetised behaving rats

Maki Kagohashi [a,b], Taizo Nakazato [a,c,*], Kenji Yoshimi [a,b], Shunjiro Moizumi [a], Nobutaka Hattori [b], Shigeru Kitazawa [a,c]

[a] *Department of Physiology, Juntendo University School of Medicine, Hongo 2-1-1, Bunkyo-ku, Tokyo 113-0033, Japan*
[b] *Department of Neurology, Juntendo University School of Medicine, Hongo 2-1-1, Bunkyo-ku, Tokyo 113-0033, Japan*
[c] *CREST, Japan Science and Technology Agency, Honcho 4-1-8, Kawaguchi-shi, Saitama 305-8575, Japan*

Received 6 August 2007; accepted 25 September 2007
Available online 3 October 2007

Available online at www.sciencedirect.com
ScienceDirect
Neuroscience Research 60 (2008) 120–127
Neuroscience Research
www.elsevier.com/locate/neures

Technical note

Wireless voltammetry recording in unanesthetised behaving rats

Maki Kagohashi [a,b], Taizo Nakazato [a,c,*], Kenji Yoshimi [a,b], Shunjiro Moizumi [a], Nobutaka Hattori [b], Shigeru Kitazawa [a,c]

[a] *Department of Physiology, Juntendo University School of Medicine, Hongo 2-1-1, Bunkyo-ku, Tokyo 113-0033, Japan*
[b] *Department of Neurology, Juntendo University School of Medicine, Hongo 2-1-1, Bunkyo-ku, Tokyo 113-0033, Japan*
[c] *CREST, Japan Science and Technology Agency, Honcho 4-1-8, Kawaguchi-shi, Saitama 305-8575, Japan*

Received 6 August 2007; accepted 25 September 2007
Available online 3 October 2007

Abstract

In vivo voltammetry is a valuable technique for rapid measurement of dopamine in the brain of freely behaving rats. Using a conventional voltammetry system, however, behavioural freedom is restricted by cables connecting the head assembly to the measurement system. To overcome these difficulties, we developed a wireless voltammetry system utilizing radio waves. This system consisted of a potentiostat and transmitter system that was mounted on the back of the rat, and a receiver and analysis system. A single-step pulse (100–250 mV) was applied at 4 Hz after an activation pulse to a carbon fibre recording electrode (diameter: 7 μm). Measurement of dopamine (detection limit: 2.7×10^{-7} M) was demonstrated *in vitro*. *In vivo* experiment was performed at least 1 week after the recording electrode was implanted in the rat striatum. Administration of 2-phenylethylamine to rats increased dopamine signal current, which was consistent with the result in the microdialysis measurement. During a resident–intruder test, dopamine signal current in a resident rat increased upon introduction of an intruder rat. These results show that the present wireless system is useful for a long-term measurement of dopamine in behaving rats.

Keywords: In vivo voltammetry; Telemetry; Cordless; Remote; Dopamine; Social interaction; 2-Phenylethylamine

1. Introduction

In vivo voltammetry has become a powerful method of recording changes in extracellular transmitter concentration in unrestrained animals (Kissinger et al., 1973; Horikawa et al., 1997; Hoffman and Gerhardt, 1998; Crespi et al., 2001; Hopwood and Stamford, 2001; Robinson et al., 2001), allowing examination of amounts of extracellular transmitter similar to microdialysis, but with higher time resolution. With recent increases in time resolution and the demonstration of stable recording over very long-term studies (>1 year; Nakazato and Akiyama, 2002; Nakazato, 2005), in vivo voltammetry has become an important recording technique in studies of learning (Richardson and Gratton, 1996; Roitman et al., 2004; Nakazato, 2005) and drug addiction (Kiyatkin and Stein, 1994, 1995; Phillips et al., 2003; Cheer et al., 2007).

One of the remaining limitations with both conventional voltammetry and microdialysis is the presence of cables connecting the head assembly to the measuring system. The widely used phrase "freely behaving animals" includes the caveat "insofar as the cables connecting the head assembly to the measurement system allow" for conventional voltammetry and microdialysis systems. Specifically, these cables prohibit recording under conditions that may introduce mechanical noise (e.g., very active movement), restrictive twisting of or damage to the cables (e.g., another animal chewing or becoming tangled), or movement through a tunnel or running wheel.

To address these problems, De Simoni et al. (1990) developed a telemetry voltammetry system using optoelectronic transmission, and measured 3,4-dihydroxyphenylacetic acid (DOPAC) and 5-hydroxyindole-3-acetic acid (5HIAA) every 2 min. Imeri et al. (1994) applied the same system to study the sleep–wake cycle in the serotonergic system for 24 h in the rat. The system used two-way wireless interconnections, one for sending the voltage ramp for oxidation from a main unit (on a desk) to a satellite unit (on the animal) and the other for sending measured current from the satellite to the main unit. However, Crespi et al.

* Corresponding author at: Department of Physiology, Juntendo University School of Medicine, Hongo 2-1-1, Bunkyo-ku, Tokyo 113-0033, Japan. Tel.: +81 3 5802 1027; fax: +81 3 3813 4954.
E-mail address: nakazato@med.juntendo.ac.jp (T. Nakazato).

0168-0102/$ – see front matter
doi:10.1016/j.neures.2007.09.011

(2004) pointed out that the two-way design would cause variations of voltage at the level of the recording electrode when the first-way channel was interrupted. The susceptibility to the interruption in the first channel would inhibit the system to work stably at a higher sampling frequency.

Two more wireless voltammetry systems were developed in 2004, one using Bluetooth digital telemetry (Garris et al., 2004) and another using infrared transmission (Crespi et al., 2004). In both systems, oxidation waveforms were generated in the satellite unit on the animal side, and consequently much better temporal resolution of 100 ms was achieved. The first one (Garris et al., 2004) was sensitive to dopamine using fast scan cyclic voltammetry, and was used in experiments with an anesthetised rat. However, the system was a large prototype that was mounted on a board of 23 cm × 19 cm, and thus was not actually mounted on a behaving animal.

The second (Crespi et al., 2004) was very small and lightweight, was sensitive to both dopamine and serotonin using chronoamperometry and differential pulse voltammetry, and recorded stable signals in experiments with rats. However, the system was not actually applied to *in vivo* measurements in awake behaving animals. Because of the use of infrared transmission, the system was vulnerable to the interruption of the infrared transmission when an obstacle, such as a hand, was interposed between the main and the satellite system (Crespi et al., 2004).

In this study, we aimed at developing a wireless voltammetry system that would be small and light enough to be fixed to an unanesthetised behaving rat, while maintaining high sensitivity to dopamine, sub-second time resolution, and very long-term (for several months) capability of a conventional wired voltammetry system that we developed in our laboratory (Nakazato and Akiyama, 1999). To overcome difficulties in the previous wireless systems, we generated voltage waveforms in a remote unit on the animal and used radio waves, rather than the infrared radiation, to mediate measured current from the remote unit to a home-base unit.

In the present report, we describe the wireless system and demonstrate the performance of the system first in the measurement of dopamine *in vitro*, second in the measurement of changes in dopamine *in vivo* in rats in response to administration of a releaser of dopamine, and lastly in the measurement of changes in dopamine in response to the introduction of an intruder rat (resident–intruder test).

2. Materials and methods

2.1. Wireless voltammetry system

2.1.1. Hardware

The system consisted of two systems, a potentiostat and transmitter system (a remote system) that carried out voltammetry with recording, reference and auxiliary electrodes, and a receiver and analysis system (a home-base system) that received data sent out from the remote system (Fig. 1). On the remote system, the voltage potential was applied to a carbon recording electrode via a potentiostat unit. Controlling signals were sent to the potentiostat from the CPU (PIC16F876; Microchip Technology Inc.) via a digital–analogue converter (AD557; Analogue-Devices Inc., Japan; Fig. 1B). The specific voltage potential was applied between the references and recording electrodes. The resulting

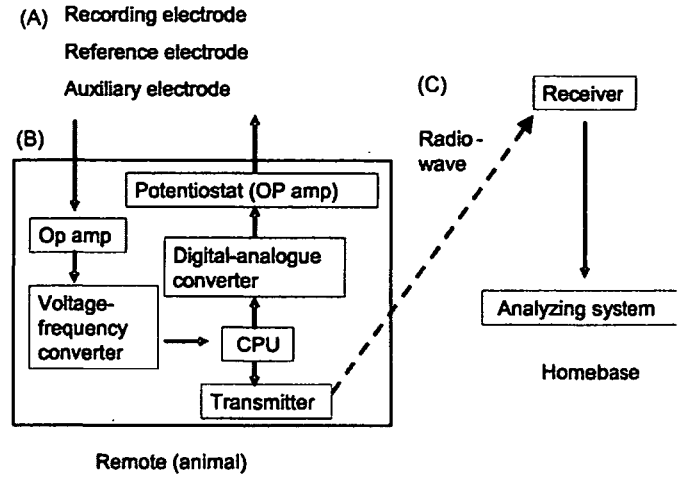

Fig. 1. Diagram of the wireless voltammetry system. (A) A recording electrode, a reference electrode, and an auxiliary electrode were placed in the recording chamber with 100 ml PBS *in vitro* or in the rat brain *in vivo*. (B) Remote system. Digital signals from the CPU were converted to analogue voltage by a digital–analogue converter. The specific voltage potential was applied using a potentiostat between the references and recording electrodes. The resulting current was converted to voltage via an operational amplifier, and then changed to pulses via a voltage–frequency converter. The pulse frequency was calculated by the CPU and transmitted by the transmitter as a radio signal. (C) Home-base system. The transmitted signal was received using a radio-wave receiver, and the data were analyzed using a microcomputer.

current (signal current) was converted to voltage via an operational amplifier (Intersil, CA, USA), and then changed to pulses via a voltage–frequency converter (AD654; Analog-Devices Inc.). The pulse frequency was calculated by the CPU and then transmitted as a radio wave between 259.45 and 264.85 MHz with a channel interval of 50 kHz (HRF-260T; Hertz Electric Co., Japan). The signal was received remotely via a CPU-controlled receiver (HRF-260R; Hertz Electric Co., Japan) that was connected via an RS-232C interface to a computer for data analysis (Fig. 1C). All electronic parts of the remote portion of the system were powered by a rechargeable battery (7.2 V, NP-FF51; Sony, Japan) that allowed for more than 8 h of continuous measurements before requiring recharging. The remote system consisted of two parts, each size was 7 cm × 4 cm × 2 cm (Fig. 2A), and the total weight with the battery was 90 g. The remote system was mounted on the back of the animal by inserting each part into a pair of bags on a harness (Fig. 2C).

2.1.2. Measurement of dopamine signal current

The paradigm used to measure dopamine signal current was as described previously (Nakazato and Akiyama, 1997, 1999). It consisted of a square-wave activation pulse (±2000 mV) and then a single-step measurement pulse (Fig. 3). The activation and measurement pulses were applied every 250 ms during measurements. To measure dopamine signal current, the potential was maintained at 100 mV and then stepped to 250 mV. Chemicals electrochemically oxidized between 100 and 250 mV were detected as the subtraction of the current at 100 mV from that of 250 mV (inset, Fig. 3). It is worth noting that chemicals other than dopamine, such as DOPAC and ascorbate, would be oxidized in the voltage range. By using these parameters, however, the ratio of *in vitro* sensitivity to dopamine, DOPAC and ascorbate is reported to be around 2000:20:1 (Nakazato and Akiyama, 1997). Thus, if the same amount of dopamine, DOPAC and ascorbate increased in a short-time period, changes in the subtracted signal current largely reflect increase in dopamine. Accordingly, we term the subtracted current as dopamine signal current.

2.2. In vitro voltammetry measurement

The recording electrode consisted of a pulled glass capillary tube containing a carbon fibre (7 μm in diameter, Toho Tenax Co., Tokyo, Japan; 500 μm of carbon fibre protruded from the pulled capillary tube tip) (Nakazato and Akiyama, 1997). The electrodes were initially activated (polished) *in vitro*

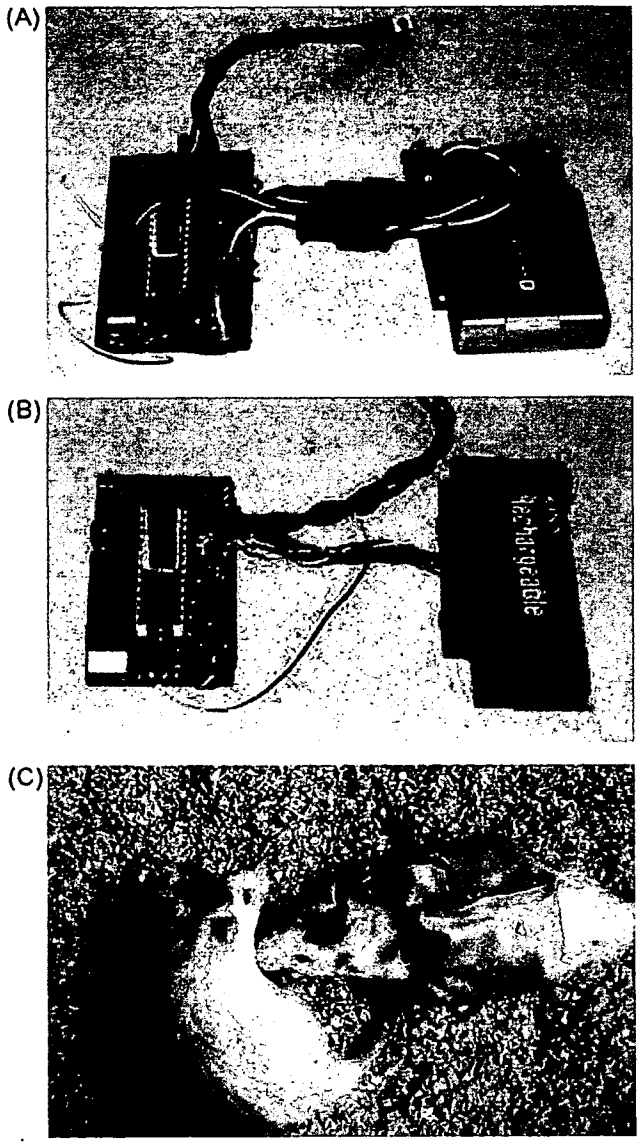

Fig. 2. Photographs of the wireless voltammetry systems. (A) Photograph of the standard remote system. The dimensions were 7 cm × 4 cm × 2 cm, and it weighed 90 g with an 8 h life rechargeable battery. All experiments were performed using this system. (B) A smaller model (5.5 cm × 3 cm × 1.5 cm, 44 g) with a 4 h life rechargeable battery. (C) The standard model placed on the back of the rat during the resident–intruder test. The circuit board and the battery were placed in the right and left pockets of the jacket, respectively.

using the conventional voltammetry system as previously described (Akiyama et al., 1985). The reference electrode was made of Ag/AgCl, and the auxiliary electrode was made of platinum wire.

In vitro electrochemical current was recorded via a recording electrode inserted into a recording chamber filled with 100 ml of 0.1 M phosphate buffered saline (PBS; pH 7.4). A reference electrode and an auxiliary electrode were also in contact with the fluid in the recording chamber. Dopamine (Sigma, St. Louis, MO, USA) was used.

2.3. *In vivo voltammetry measurement*

2.3.1. *Subjects*

Male Wistar rats (350–400 g; $n = 11$) were purchased from Charles River Laboratories (Yokohama, Japan). The animals were housed one to four per cage, fed with solid food (MF, Oriental Yeast Co. Ltd.) with water available *ad libitum* and maintained on a 12 h light–dark cycle at constant temperature and humidity.

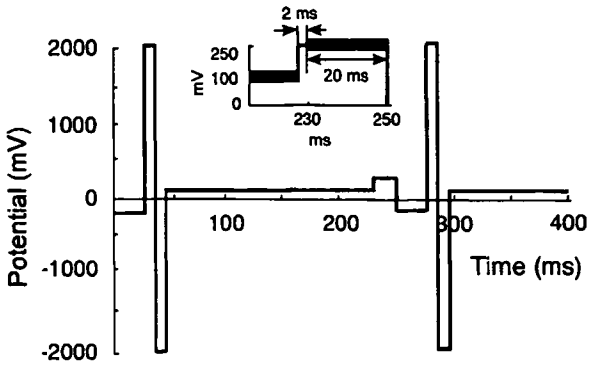

Fig. 3. Potential paradigm for measurement of dopamine signal current. After a 2 ms interval, signal current was measured 40 times during the time indicated by the thick line (20 ms) in the insets, and averaged. The potential was stepped from 100 to 250 mV.

Animals were cared for in accordance with Guiding Principles for the Care and Use of Animals approved by the Council of the Physiological Society of Japan, and all experiments were approved beforehand by the Committee for Animal Experimentation of Juntendo University School of Medicine.

2.3.2. *Animal preparation*

Rats were anesthetised using pentobarbital (50 mg/kg, i.p.) and holes were drilled in the skull for chronic placement of a recording electrode, reference electrode, and auxiliary electrode (Nakazato and Akiyama, 2002). The recording electrode was placed unilaterally into the striatum (AP: 0, ML: +3, DV: +5.5 from the surface of the dura mater; Paxinos and Watson, 1986). The reference electrode was placed on the dura mater, and the auxiliary electrode was anchored to the skull. These electrodes were fixed to the skull using dental cement for chronic experiments.

Dopamine signal currents were measured more than 1 week after the implantation of the electrodes and they were active for several months. Before each measurement, the wireless system was placed on the back of the rat (Fig. 2C).

2.3.3. *Drug administration*

The dopamine releaser 2-phenylethylamine (PEA; Sigma, St. Louis, MO, USA), one of the trace amines, was dissolved in normal saline and injected subcutaneously at a dose of 100 mg/kg ($n = 5$). Changes in dopamine signal current were measured using the wireless voltammetry system. The data were sampled at 4 Hz. The results were compared with those obtained using the conventional hard-wired voltammetry system that has been used in many experiments in our laboratory (Nakazato and Akiyama, 1997, 2002). Using the conventional system, dopamine signal current was measured every 2 min.

2.3.4. *Resident–intruder test*

Male Wistar rats ($n = 4$) were reared in separate home cages (50 cm × 30 cm × 30 cm). The effects of social interaction between two rats were examined. The difference in body weight of these rats was less than 20 g. Before the experiments, the wireless voltammetry system (remote system) was mounted on the back of the resident rat under isoflurane anesthesia. The resident rat started moving in the cage 1–2 min after the procedure. Then, more than 1 h later, the intruder rat was introduced for approximately 5 min into the resident rat's home cage, and dopamine signal current was measured during the time of the encounters.

2.3.5. *Data analysis*

We excluded outliers in the measured dopamine signal current in a following manner. First, differences between adjacent elements of data were calculated and data points that fell outside the range of 5 S.D. around the mean difference were removed. The data was then smoothed by a moving average method (width of 2 min, phase corrected) and deviations from the smoothed data were calculated. Outliers that fell outside the 5 S.D. range around the smoothed data were removed. Zero to 1.3% of data points (0.37 ± 0.42%; mean ± S.D.) were excluded in a total of 12 experiments. After excluding